Received: 14 February 2023 | Revised: 3 October 2023 | Accepted: 6 December 2023

DOI: 10.1002/cta.3914

ORIGINAL PAPER

WILEY

Enhancement of photovoltaic array characteristics and global maximum power using Padovan transform-based image encryption strategy

Kanasottu Anil Naik[1] | **Rayappa David Amar Raj**[1] | **Thanikanti Sudhakar Babu**[2] | **Belqasem Aljafari**[3]

[1]Department of Electrical Engineering, National Institute of Technology, Warangal, India

[2]Department of Electrical and Electronics Engineering, Chaitanya Bharati Institute of Technology, Hyderabad, India

[3]Department of Electrical Engineering, College of Engineering, Najran University, Najran, Saudi Arabia

Correspondence
Rayappa David Amar Raj, Department of Electrical Engineering, National Institute of Technology, Warangal, India.
Email: dtcdavid2k15@gmail.com

Summary

During shading, the mismatch between the panels in the photovoltaic (PV) array mitigates the global maximum power (GMP). Besides, the mismatch in the irradiation levels of distinct rows of the PV array instigates multiple power peaks (MPPs) in the array characteristics. Distinguishing the local and global peaks among MPPs for tracking the GMP is highly challenging for maximum power point tracking (MPPT) controllers. So, to mitigate the MPPs and enhance the GMP, array reconfiguration is preferred. Nevertheless, most existing reconfiguration techniques exhibit poor shade dispersal, distorted electrical characteristics, multiple MPPs, increased mismatch, scalability issues, etc. To overcome these challenges, this paper proposes a new Padovan transform-based encryption strategy for array reconfiguration. The proposed method was evaluated for both symmetric and unsymmetrically sized arrays. Its performance has also been compared to that of 23 other strategies. The proposed reconfiguration strategy integrated with MPPT is validated experimentally using a prototype model. A nonparametric statistical hypothesis test with a *p*-value of 0.05 has been used for a pairwise fair comparison study among the examined approaches. The proposed approach constantly outperforms the current methods because of its unique shade dispersion generated through intelligent reconfiguration offering the GMP improvement of 34.429%, 12.51%, 5.05%, and 37.40%, 22.93%, 16.51% for 9×9 and 4×8 PV arrays, respectively.

KEYWORDS

global maximum power, image encryption, mismatch, multiple power peaks, Padovan series, reconfiguration

1 | INTRODUCTION

Partial shadowing (PS) is a typical and common occurrence experienced by photovoltaic (PV) panels. The electrical properties of the PV panels are altered when they are shaded. Mismatch losses occur when the characteristics of the panels of the array differ, resulting in a mismatch.[1] Because of shadowing, the shaded panel serves as a power sink, whereas the unshaded ones serve as a power source. The massive accumulation of currents at the shaded part causes

the formation of hotspots, which can lead to fire-related hazards. To overcome these negative consequences, protection diodes that bypass the current during PS should be incorporated. These diodes, on the other hand, cause a lot of peaks distorting the array characteristics.[2] Because of the multiple local and global power peaks (MPPs), an efficient maximum power point tracking (MPPT) algorithm[3] is required to operate the PV array at global maximum power (GMP). Nonetheless, simple and traditional MPPT approaches may get stuck in the local maxima, resulting in sub-optimal output. As a result, an effective MPPT controller is necessary to extract the GMP, and numerous novel approaches have been proposed. An enhanced P&O MPPT approach for a two-stage grid-connected PV system with effective open-circuit voltage estimate is proposed and tested under realistic solar radiation.[4] A global MPPT algorithm using modified honey badger optimization for triple-junction PV system is proposed to track the GMP under partial shading condition.[5] Recently, a new three-stage current-mode MPPT strategy with fixed and varying current-perturbation steps is proposed in Sousa et al.[6] to track the optimal MPP and enhance its robustness and performance. However, regardless of their sophistication, these controllers are incapable of extracting the array's full capacity and can only track its GMP. Furthermore, array reconfiguration is preferred to improve the array output even further than what can be achieved by using the MPPT alone.

The detailed literature review on state-of-the-art PV array reconfiguration strategies with their pros and cons is presented in Table 1. Based on the way of functioning, reconfiguration techniques are generally categorized as static and dynamic. Electrical array reconfiguration (EAR),[7,8] artificial intelligence (AI),[9,10] and metaheuristic-based[11–17] approaches are the three main types of dynamic strategies. The AI-based solutions reduce mismatch losses, but they include both static and adaptive sections of an array, with only the adaptive section being able to be changed, failing to find the best solution. Furthermore, they necessitate a large number of switches, a switching matrix, advanced control mechanisms, sensors, driver circuits, and other components, making the solution extremely expensive. Furthermore, the fuzzy approaches use a lot of memory to operate the switching matrix. The aforementioned devices are also used in EAR-based techniques for proper operation, and implementing EAR for larger PV farms is quite difficult. They also generate a large number of switching pulse patterns in order to find the best one. A recent rise in the popularity of metaheuristic-based algorithms can be attributed to their success in creating switching matrix structures for dynamic array reconfiguration. However, all of these algorithms have serious issues, including lengthy computation times, convergence process issues, a variety of parameters, parameter selection difficulties, tuning parameter and weighting factor issues, the likelihood of getting stuck at local maxima, a large search space, numerous iterations, complex algorithms, the use of unpredictability, and more than one stage to solve. Hence, the one-time/fixed/static reconfiguration approaches are recommended because of the aforementioned problems and practicality issues associated with dynamic reconfiguration.

Static reconfiguration techniques, unlike the dynamic ones, do not necessitate sensors, switching matrices, switches, or any other associated devises to operate, making them a cost-effective alternative for mitigating the impacts of partial shading. Nevertheless, as shown in Table 1, many of the available static approaches have several limitations. Scalability concerns, indiscriminate shade distribution, various solution sets, increased mismatch in rows, inconsistent performance, and a large number of MPPs in the array characteristics are limitations that the previous solutions inherit which burdens the MPPT systems to distinguish the local and global optimum. To address all the aforementioned shortcomings, a Padovan transform-based reconfiguration approach using the well-known Padovan sequence is proposed. This proposed work's novel aspects and main contributions are as follows:

- A very effective, uncomplicated, scalable, switchless, sensor-less integer series-based solar array reconfiguration strategy is provided to effectively distribute the shade, and the effectiveness of this approach is assessed using image quality indices.
- The proposed Padovan transform (PT) approach intelligently disperses the shade, unlike numerous static approaches that indiscriminately distribute the shade. This is accomplished by the intelligent property of the PT technique, which reduces the correlation between neighboring shaded panels of an array in a column, row, and diagonal, hence increasing the total irradiation of a specific row of an array.
- The proposed technique, unlike many static reconfiguration strategies, is scalable for any sizing of PV array and has been validated for various sizes such as 9×9, 4×4, and 4×8.
- The performance of the proposed PT is compared with the 23 static reconfiguration strategies that were recently developed.
- A detailed pictorial comparative row current variation analysis of various configurations under distinct shading cases is presented.

TABLE 1 Literature review on state-of-the-art PV array reconfiguration strategies.

Ref	Approach	Category	Size	Description	Related problems
[7]	Dynamical EAR	EAR, Dynamic	3 × 2	Electrical reconfiguration by inserting an adjustable switching matrix between PV array and inverter	Employs communication matrix, data acquisition system, data recorder, monitoring system, complex controlling unit, numerous switches and sensors
[8]	Dynamic		2 × 2	Introduced dynamic reconfiguration approach for water pumping	Large-scale feasibility is difficult to achieve since it necessitates the coordination of several switches
[9]	Neural network (NN)	AI, Dynamic	3 × 4	Used NN approach to coordinate adaptive and fixed parts of array to equalize row irradiation	Utilizes various sensors, switches, and controller units but falls short of offering the best solution
[10]	Fuzzy related		3 × 4	Reconfiguration based on the partial shadowing detection	For detection and reconfiguration, switches, sensors, switching matrix, and a complicated algorithm are required.
[11]	Genetic algorithm (GA)	Metaheuristic, Dynamic	9 × 9	Finds optimal switching pattern using GA algorithm for maximizing GMP	Parameter selection difficulty, weighted-sum approach, convergence issues, may traps at local optimum
[12]	Particle swarm optim.		9 × 9	Obtains optimal switching pattern using PSO method for mitigating MPPs	Easily stuck in local maxima, tunning parameter issues, weighted-sum approach
[13]	Butterfly optim.		9 × 9	Implemented to distribute the shade requiring few parameters in methodology	Tested only under one type (diagonal) of shading conditions, quite limited analysis
[14]	Grey wolf optim.		9 × 9	Enhances the GMP by minimizing row current variation solving as a multi-objective problem	Weighted-sum method, choosing the wrong weights yields a less than ideal result
[15]	Grasshopper optim.		9 × 9	Finds the optimal reconfigured matrix pattern for a particular shading condition	Complex computation, inconsistent behavior, low convergence, easily trapped in local maxima
[16]	Two-step GA		9 × 9	Changes to electrical circuit connections are made using a two-stage reconfiguration method based on GA	Complex algorithm involving two stages in reconfiguration, suffer GA methodology drawbacks
[17]	Artificial ecosystem		9 × 9	Attains uniform shade dispersion employing less parameters	Complex methodology, contains random parameters values resulting in lower output
[18]	Sudoku (SP)	Puzzle-based, static	9 × 9	PV array reconfiguration based on SP pattern to increase GMP extraction	Incompatible for unsymmetrical array sizes, there are various solution sets, Finding the ideal pattern is not practical.
[19]	Futoshiki puzzle (FT)		9 × 9	Implemented FT-based shade dispersion to obtain better array characteristics	Not scalable to unsymmetrical arrays, inconsistent performance, exists many solution sets
[20]	Shift modified (ST)	Shift-based, static	9 × 9	physically repositions panels in an array while maintaining electrical circuitry	Failed to validate the effectiveness of algorithm for unsymmetrical arrays
[21]	Column index (NC)		9 × 9	Fixed and one-time reconfiguration approach employed to mitigate the mismatch losses	Methodology not tested for unsymmetrical PV arrays; very limited analysis performed

TABLE 1 (Continued)

Ref	Approach	Category	Size	Description	Related problems
[22]	Optimal Sudoku arrangement (OPS)	Puzzle-based, Static	9 × 9	Modified version of sudoku puzzle pattern applied to 9 × 9 PV array to disperse the shade	Difficulties with compatibility, same SP method restrictions, variable performance
[22]	Non-optimal Sudoku (NO)		9 × 9	Employs additional rules to the Sudoku rules to find rearranged pattern	Same limitations as that of SP, not scalable for asymmetric array sizes
[23]	Latin square (LAS)		4 × 4	Physical panel relocation for TCT-configured array employing LAS pattern	Improper diagonal shading distribution of shade, unable to support asymmetrical arrays
[24]	Improved Sudoku (IS)		9 × 9	Relocation based on improved Sudoku-puzzle pattern for minimizing MPPs	Disadvantages similar to those of the SD approach, performance issues when experiencing diagonal shading
[25]	Skyscraper (SK)	Puzzle-based, static	9 × 9	Uses skyscraper puzzle pattern to lessen protection diodes losses	Fails when shading is diagonal, difficulties with compatibility, many solution sets exist
[26]	Lo Shu puzzle (LP)	Magic-square, static	9 × 9	Employs shadow dispersion based on the Lo-Shu grid for augmenting array's electrical characteristics	Not compatible to all arrays, cannot be applicable to other than $3n \times 3n$ arrays, variable performance
[27]	Diagonal-arrangement (DA)	Logic-based, static	9 × 9	To spread the row shading the method arranges all of the panels diagonally	Yields poor performance because of correlation among diagonal panels of an array
[28]	Magic square (MGS)	Magic-square, static	4 × 4	Mitigates the row mismatch based on magic-square pattern under low irradiation conditions	Lacks effective shade dispersion, not scalable to unsymmetrical arrays
[29]	Odd-even (ODE)	Number-based, static	6 × 4	Proposed analytical strategy for reconfigured matrix using odd and even numbers	Poor shade dispersion results from the remaining half of the panels being in the same row, displays a lot of MPPs, frequently performs below expectations
[30]	Optimal Sudoku (OS)	Puzzle-based, static	9 × 9	Reconfigures the conventional total cross tied array configuration based on OS technique	Unable to work with all arrays, many solution sets exist, Finding the ideal configuration is not feasible.
[31]	Odd–even prime (OEP)	Number-based, static	9 × 9	Extended version of ODE incorporating prime elements in obtaining reconfigured matrix	50% of the panels remain in the same rows, exhibits numerous MPPs, inconsistent performance
[32]	Diagonal TCT (DIT)	Shift-based, static	4 × 4	Reconfigures the conventional TCT-configured array based on shifting operations	Displays extremely low performance in circumstances of diagonal and other shadings, low-GMP improvement
[33]	Multi-diagonal Sudoku (MS)	Puzzle-based, static	9 × 9	Based on the multi-diagonal Sudoku arrangement this technique configures the panels	Poor shade distribution under some shadings, unable to scale for asymmetrical arrays
[33]	Canonical Sudoku (CS)		9 × 9	Canonical Sudoku pattern-based physical relocation of panels	Significant row current mismatch, inconsistent performance, compatibility issues
[34]	Advanced Sudoku (AS)		9 × 9	Physical relocation of panels based on the advanced variant of Sudoku pattern	Not applicable for asymmetric arrays, exists numerous solution sets

(Continues)

TABLE 1 (Continued)

Ref	Approach	Category	Size	Description	Related problems
[35]	Henon map (HEM)	Chaotic-based, static	9 × 9, 3 × 5	Minimizes row current mismatch using a Henon chaotic map for array restructuring	Not effective under column shading, low GMP enhancement
[36]	Spiral pattern array (SPP)	Pattern-based, static	9 × 9	PV array rearranged to maximize GMP using spiral-step design	Poor reconfiguration strategy, ineffective under diagonal shading, not scalable
[37]	Twisted two-step	Repositioning, static	9 × 9	Reconfigures the array by swapping the panels in z sequence to mitigate mismatch	During column shading there is poor shade dispersion, underperforms in many shady situations
[38]	Chaos map (CAM)	Chaotic-based, static	6 × 6 7 × 7	Switchless and sensor less method inspired by image processing	Cannot be applicable for unsymmetrical arrays, poor shade dispersal, exhibit several MPPs

- A laboratory experimental prototype of the proposed configuration was developed and tested using conventional MPPT controller under distinct shading conditions.
- To verify the consistency and reliability of the new technique statistically compared to the current ones, a pairwise unbiased comparison analysis utilizing a nonparametric statistical Wilcoxon signed rank sum test with a significance of 0.05 is conducted.

2 | PADOVAN TRANSFORM-BASED IMAGE ENCRYPTION STRATEGY

An integer sequence is an ordered set of integers in mathematics. It can be explicitly defined by giving a formula to its m^{th} term, or it can be defined inferentially by showing a relationship between its terms. There are several such integer sequences, with the Padovan sequence[39] being one of the most well-known which is described as follows:

2.1 | Padovan series and its transform

The Padovan sequence $(P_n)_{n\geq 0}$ named after the architect Padovan is a ternary recurrence relation[40] defined as

$$P_n = \begin{cases} 1 & \text{if } n = \{0,1,2\} \\ P_{n-2} + P_{n-3} & \text{if } n \geq 3 \end{cases} \tag{1}$$

with the initial conditions $P_0 = 0, P_1 = P_2 = 1$. The first few terms of Padovan sequence are

n	0	1	2	3	4	5	6	7	8	9	10	11	12	.....
P_n	1	1	1	2	2	3	4	5	7	9	12	16	21	.....

It is noted that the first three terms of the series are 1 and then from the fourth term, each term is the sum of one but preceding two terms, that is, fourth term is the sum of the second and the first terms of the sequence; the fifth term is the sum of third and second terms and so on. The ratio of n^{th} term to the $(n-1)^{\text{th}}$ term in the Padovan series as $n \to \infty$ is called limiting ratio "τ",[41] which is by definition as

$$n \to \infty, \frac{P_n}{P_{n-1}} = \tau.$$

As $n\to\infty$, $\frac{P_n}{P_{n-3}}=\frac{P_n}{P_{n-1}}\times\frac{P_{n-1}}{P_{n-2}}\times\frac{P_{n-2}}{P_{n-3}}=\tau\times\tau\times\tau=\tau^3$ and from Equation (1), we can write

$$P_{n+3}=P_{n+1}+P_n \tag{2}$$

By dividing Equation (2) by P_n, we get

$$\frac{P_{n+3}}{P_n}=\frac{P_{n+1}}{P_n}+1\Rightarrow\ \tau^3=\tau+1 \tag{3}$$

The characteristic equation, $\tau^3-\tau-1=0$, in Equation (3) has roots α, β, $\gamma=\overline{\beta}$,,[40] where

$$\alpha=\frac{(r_1+r_2)}{6};\beta=\frac{-(r_1+r_2)+\sqrt{-3}(r_1-r_2)}{12}$$

with $r_1=\sqrt[3]{108+12\sqrt{69}}$, $r_2=\sqrt[3]{108-12\sqrt{69}}$

Equation (3) has three roots: one real root "ρ" and two complex conjugate roots "β" and "γ." The unique positive real solution of the cubic equation in Equation (3) is known as plastic number "α" which is a mathematical constant[39] and is given as

$$\alpha=\sqrt[3]{\frac{1}{2}+\frac{1}{6}\sqrt{\frac{23}{3}}}+\sqrt[3]{\frac{1}{2}-\frac{1}{6}\sqrt{\frac{23}{3}}}=1.3247179$$

The Padovan sequence involving the roots α, β, γ[40] can be expressed by a formula (known as Binet-like formula for Padovan numbers) as follows

$$P_n=a\alpha^n+b\beta^n+c\gamma^n,\ \text{for all}\ n\geq 0 \tag{4}$$

where $a=\frac{\alpha+1}{(\alpha-\beta)(\alpha-\gamma)}$, $b=\frac{\beta+1}{(\beta-\alpha)(\beta-\gamma)}$, $c=\frac{\gamma+1}{(\gamma-\alpha)(\gamma-\beta)}=\overline{b}$

Generally, a transformation matrix is used in the image encryption approach for relocating the pixels in an image.[42] The pixels are successfully relocated by the transformation matrices created by the integer sequences. The Padovan sequence-based transform preserves uniformity by spreading all neighboring pixels in such a manner that they are all equidistant from one another, leading to enhanced encryption. It should be noted that a 2×2 matrix made up of the four successive terms of the Padovan sequence is a unimodular matrix (and it contains many of such sets) that effectively relocates a matrix's pixel coordinates and can thus be used for image processing via encryption.[43] The general form of PT is a mapping $F:T^2\to T^2$ that can be written as follows:

$$\begin{bmatrix}x(i+1)\\ y(i+1)\end{bmatrix}=\begin{bmatrix}P_i & P_{i+1}\\ P_{i+2} & P_{i+3}\end{bmatrix}\begin{bmatrix}x(i)\\ y(i)\end{bmatrix}\bmod \mathrm{N} \tag{5}$$

In Equation (5), x and $y\in\{0, 1, 2, 3, \ldots .N-1\}$, $x(i)$, $y(i)$ are the old positions and $x(i+1)$, $y(i+1)$ are the new positions of the matrix, P_i is i^{th} term in a Padovan sequence, "mod" is the modulo operation, and "N" is the size of the image. So, by using the Padovan transformation matrix, the old positions are replaced by the new ones. By denoting $\begin{bmatrix}P_i & P_{i+1}\\ P_{i+2} & P_{i+3}\end{bmatrix}$ as PT_i, the first, second, and third transformation matrices of the Padovan sequence are given as follows:

$$PT_1=\begin{bmatrix}P_1 & P_2\\ P_3 & P_4\end{bmatrix}=\begin{bmatrix}0 & 1\\ 1 & 1\end{bmatrix};PT_2=\begin{bmatrix}P_2 & P_3\\ P_4 & P_5\end{bmatrix}=\begin{bmatrix}1 & 1\\ 1 & 2\end{bmatrix};PT_3=\begin{bmatrix}P_3 & P_4\\ P_5 & P_6\end{bmatrix}=\begin{bmatrix}1 & 1\\ 2 & 2\end{bmatrix};\ldots..$$

The transformation matrix of the Padovan series can also take on numerous other forms for various "i" values. Further improving the encryption process is iterating Equation (5) with the subsequent process.

$$\begin{bmatrix} x(i+1) \\ y(i+1) \end{bmatrix} = \begin{bmatrix} P_i & P_{i+1} \\ P_{i+2} & P_{i+3} \end{bmatrix}^n \begin{bmatrix} x(i) \\ y(i) \end{bmatrix} \bmod N,\ 0\, n \geq 2 \tag{6}$$

Equilateral triangles with the edge lengths specified by the Padovan series are assembled in a spiral pattern in an anticlockwise direction as seen in Figure 1A. Further, the most remarkable aspect of the Padovan recurrence sequence is that it can be obtained from the Pascal's triangle by summing up the numbers of its diagonals, as seen in Figure 1B.

2.2 | Employment of PT approach in reconfiguration

The image is encrypted by repositioning its pixels using the 2 × 2 transformation matrix created by the Padovan series. For example, in Figure 2, the element "6" that is basically situated in (2, 3) coordinates of the original 3 × 3 matrix is

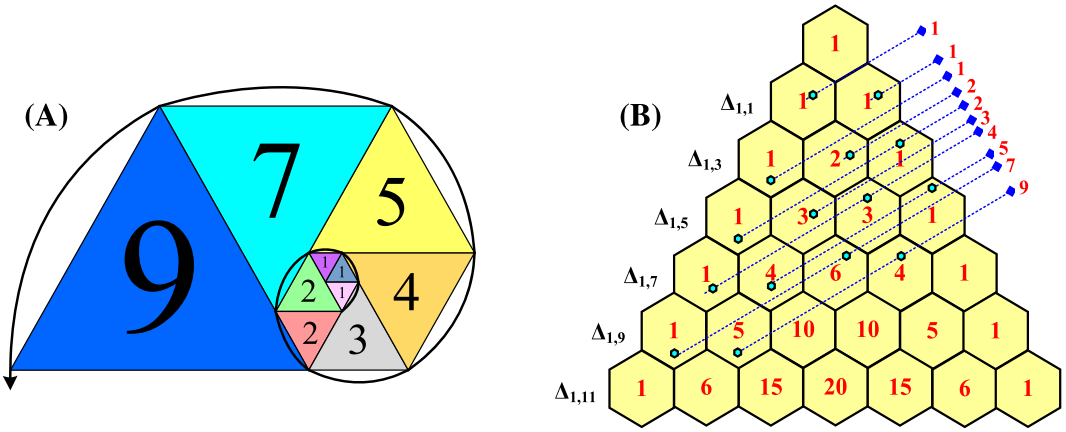

FIGURE 1 (A) Golden spiral obtained by Padovan series. (B) Pascal's triangle Padovan series mapping. [Colour figure can be viewed at wileyonlinelibrary.com]

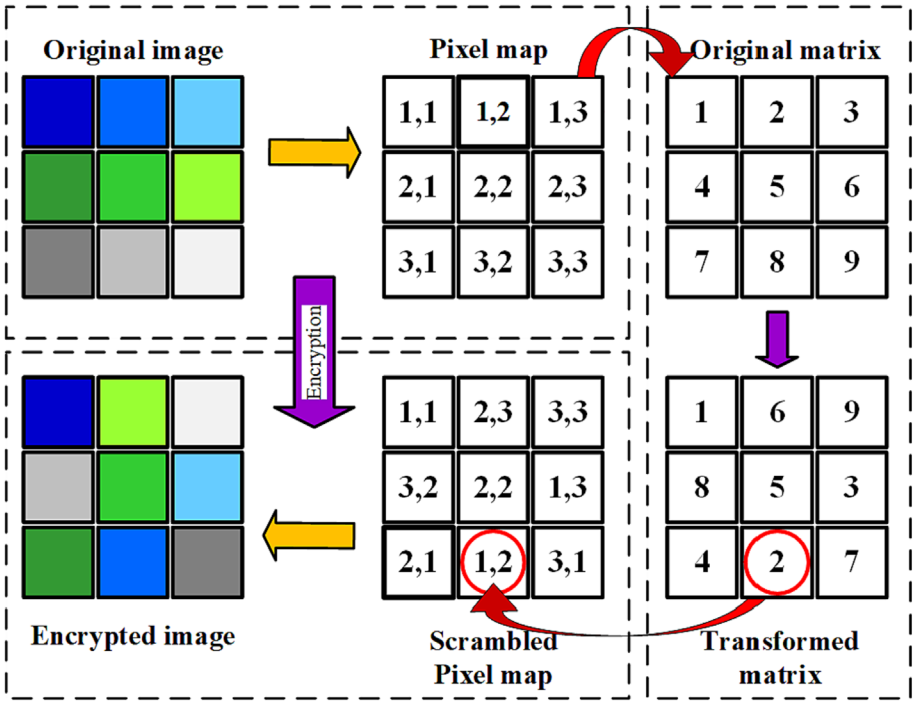

FIGURE 2 Description of image encryption process. [Colour figure can be viewed at wileyonlinelibrary.com]

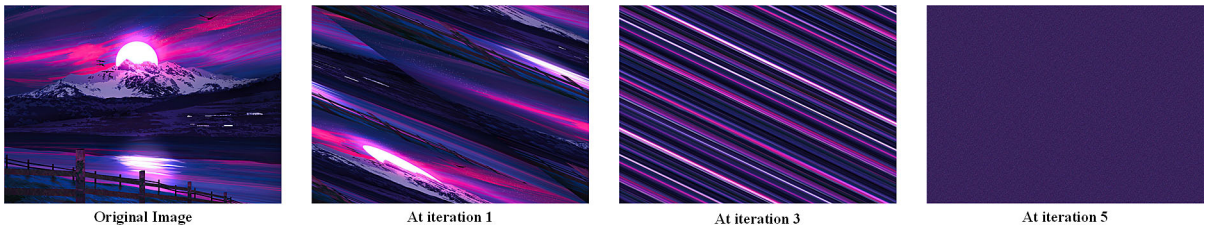

FIGURE 3 Original image and the encrypted image over the iterations obtained by PT. PT, Padovan transform. [Colour figure can be viewed at wileyonlinelibrary.com]

now relocated to (1, 2) coordinates based on the rearranged matrix obtained by the transformation matrix of the encryption algorithm. Accordingly, all the pixels in the image (matrix) are effectively repositioned to achieve the lowest correlation between the rearranged matrix's neighboring pixels. It is noted from Figure 3 that the pixels of the original image are effectively repositioned over five iterations when it is applied with the proposed Padovan transform-based (PT) encryption strategy. To produce the rated output, the solar PV array consists of solar panels coupled in parallel and series, just like the image is composed of numerous pixels clustered together. By treating each PV panel individually as a pixel and the entire PV array as the image's collection of pixels, PT based-encryption process is implemented. The PV array is configured based on the rearranged matrix pattern obtained by the PT approach for distributing the shadow equally over the array, thereby mitigating the row current fluctuation under partial shading conditions.

The PV array is optimally reconfigured using a predetermined configuration pattern derived using the PT approach without changing the electrical interconnections. This reduces the shading effect while maintaining the electrical characteristics of the array. A rearranged PT matrix directs the physical relocation of the panels of the TCT-configured array. The PV panel number 36 that is in the third row and sixth column shown in Figure 4 is now placed in the third row and second column based on the obtained PT matrix as shown in the figure. Similarly, using the generated PT matrix, all of the panels are properly reconfigured to disperse the shadow uniformly. Now, if the shade occurs in the first row of the PT-configured array with PV panel numbers 77, 61, 52, 43, 34, 25, and 16, the row shading is diffused to all rows, equalizing the irradiation between the rows because these panels are physically positioned in the first row but are electrically connected to various rows of an array. As a result, the proposed Padovan transform-based array reconfiguration approach minimizes the row-current mismatch effectively during shading conditions. The flow chart of the overall PT -based PV array reconfiguration approach is shown in Figure 4.

2.3 | Performance evaluation using image quality indices

The proposed PT intelligently and uniformly disperses all the pixels resulting in superior encryption. Because the suggested technique may be employed as an image scrambler in the picture encryption process, its efficacy can be more accurately evaluated using the image quality evaluation metrics[44] shown in Table 2. A successful encryption algorithm has the following characteristics: the least correlation, the highest mean square error (MSE), the peak signal-to-noise ratio (PSNR), and the least structural similarity index (SSIM). The degree to which the algorithm has decorrelated adjacent pixels as much as is practical can be seen in the least correlation. The highest inaccuracy between the actual and encrypted images is indicated by greater MSE and lower PSNR values. Furthermore, the smaller the SSIM, the less structurally similar the images are. All of these indicators are optimized using the proposed PT approach.

3 | CONVENTIONAL INCREMENTAL CONDUCTANCE-BASED MPPT

The PV energy is becoming increasingly popular for use in electrical power applications. It still has a low conversion efficiency, though. As a result, efficiency can be increased by utilizing high-efficiency power MPPT trackers which are developed to harvest the maximum amount of power from the PV system. Numerous MPPT methods have been proposed, including the incremental conductance (INC) method is frequently taken into consideration because of its good performance, which includes simple installation, quick tracking, and improved effectiveness. With this approach, which focuses solely on power variations, the PV panel's conductance and incremental conductance are calculated

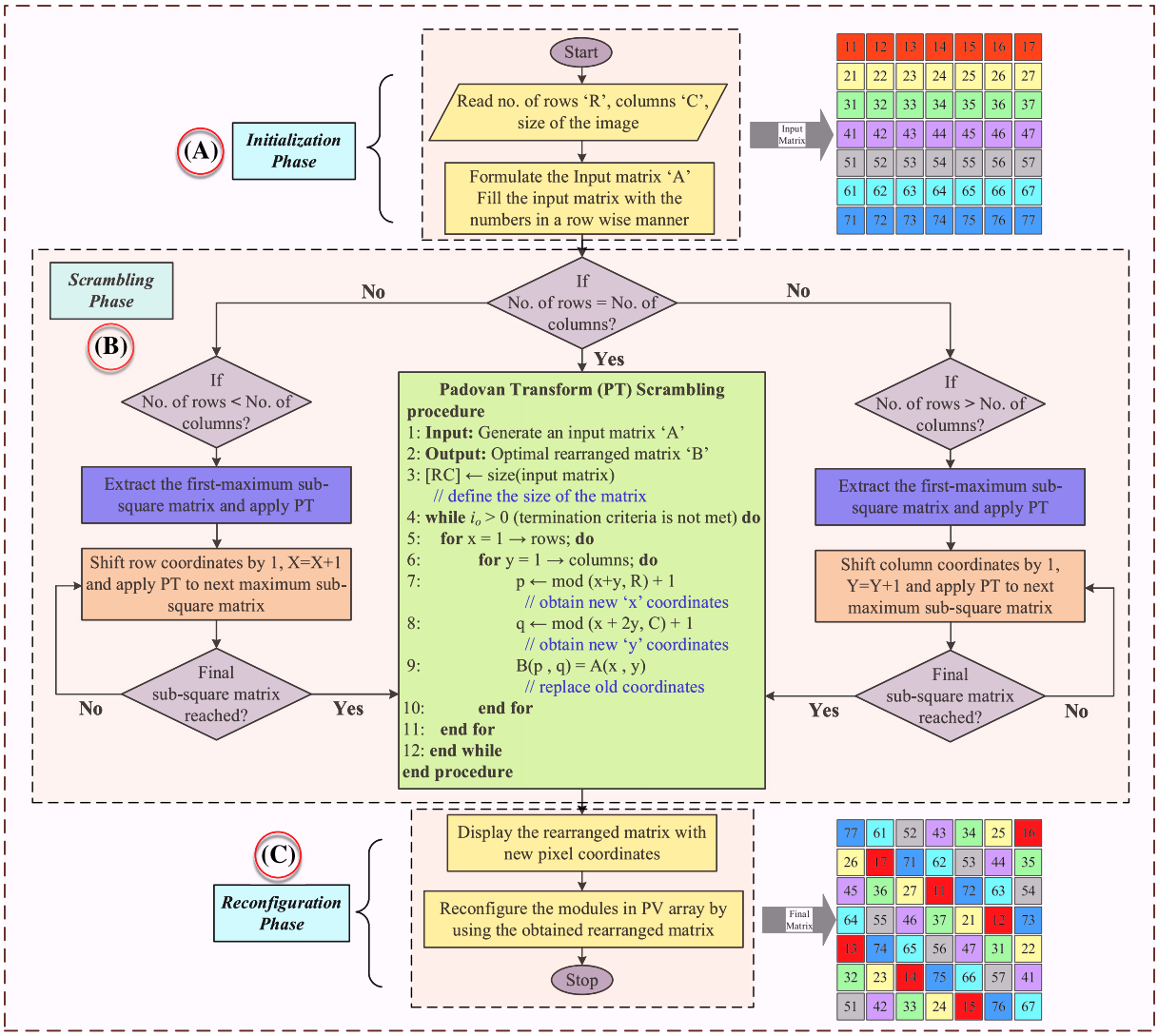

FIGURE 4 Flow chart of the overall Padovan transform-based PV array reconfiguration approach. PV, photovoltaic. [Colour figure can be viewed at wileyonlinelibrary.com]

TABLE 2 Performance evaluation of PT using image quality indices.[44]

Array	Correlation	MSE	SSIM	PSNR
9 × 9	+0.0001	1346.70	+0.0281	−31.2926
4 × 4	−0.0198	257.50	−0.0194	−24.1078
4 × 8	+0.0230	254.50	+0.0244	−24.0569

Note: MSE, mean square error; PT, Padovan transform; PSNR, peak signal-to-noise ratio; SSIM, structural similarity index.

instantly, rising to the left of the MPP and falling to the right. When the derivative of array power by voltage (dP/dV) is zero, the maximum power point (MPP) is reached. The fundamental equations of this approach are deduced from the conceptualization that the array's $P-V$ characteristics at maximum power have a slope of zero, as stated in Equation (6). Figure 5 shows the flowchart for the incremental conductance approach.[45] In this paper, we have used incremental conductance-based MPPT algorithm in Section 4.4 for tracking the GMP of the PV array.

$$\frac{dP}{dV}=0; \quad At\,GMP \tag{7}$$

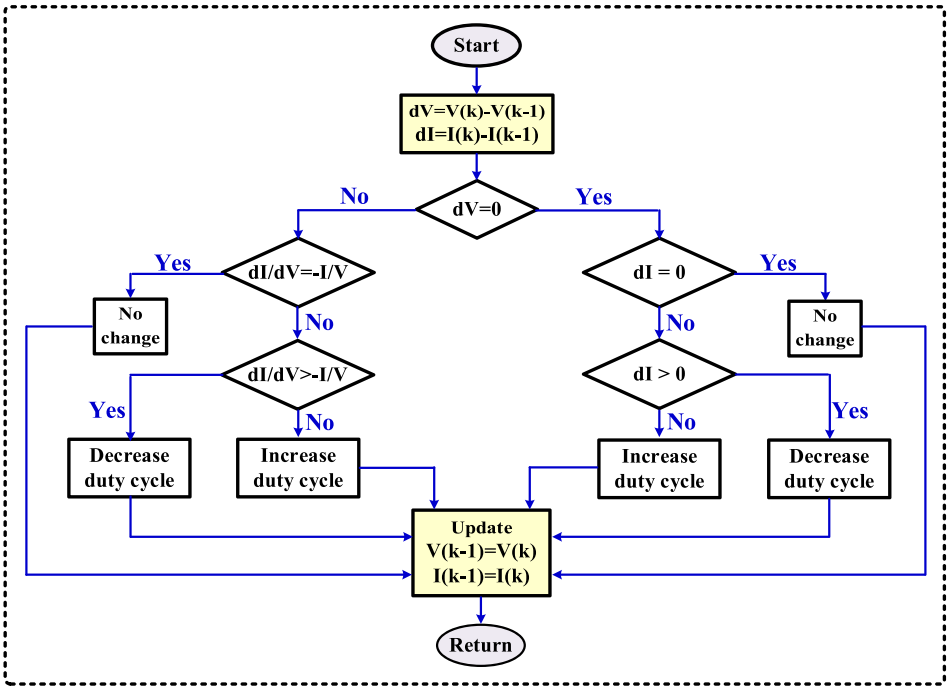

FIGURE 5 Flow chart of the incremental conductance-based MPPT algorithm. MPPT, maximum power point tracking. [Colour figure can be viewed at wileyonlinelibrary.com]

Equation (6) can be further written as

$$\frac{dP}{dV} = I\frac{dV}{dV} + V\frac{dI}{dV} \tag{8}$$

$$\frac{dP}{dV} = I + V\frac{dI}{dV} \tag{9}$$

$$I + V\frac{dI}{dV} = 0 \tag{10}$$

$$\frac{dI}{dV} = -\frac{I}{V} \quad \text{At GMP} \tag{11}$$

$$\frac{dI}{dV} > -\frac{I}{V} \quad \text{Left of GMP} \tag{12}$$

$$\frac{dI}{dV} < -\frac{I}{V} \quad \text{Right of GMP} \tag{13}$$

4 | RESULTS AND DISCUSSION

The majority of the reconfiguration strategies have experimented with their performance for a 9 × 9 symmetrical PV array under various shading conditions. So, in order to study the performance of the proposed PT strategy with respect to the existing techniques, a 12.809 kW, 9 × 9 PV array (with nominal voltage and current at P_{max} are 194.89 V and 65.722A, overall efficiency of 12.46%) is developed and analyzed in the MATLAB simulation environment. To demonstrate the effectiveness of the proposed PT, the system is investigated under five distinct shading scenarios and the

obtained results are compared to that of the available 21 techniques of 9 × 9 array. A Kyocera Solar KC175GT solar panel is considered at 900 W/m^2, 25°C in the simulation studies where the panel is assumed to receive 900 and 400 W/m^2 under normal and shading cases, respectively. The row irradiation of PV array for 9 × 9 array before and after implementation of the proposed PT strategy is shown in Table 4.

4.1 | Analysis on symmetric 9 × 9 PV array

A triangle-patterned uniform shadowing case is considered in Case 1, which limits the irradiation in the bottom half of the PV array as shown in Figure 6. In this scenario, the OS technique outperformed all other techniques that were investigated. Following the OS, the proposed PT and SPP techniques perform on par yielding an enhancement of nearly 34.5% in GMP (from Table 3). Although the existing OS has the best result in Case 1, it performs poorly in Case 2 and dramatically fails in Cases 4 and 5, dropping output by 1.73% and 4.07%, respectively, when compared to benchmark TCT. Additionally, one of OS's major limitations is that it cannot be used for asymmetric arrays. Furthermore, in this case, SPP outperforms PT by a little margin. SPP, however, fails to provide consistency, as its performance in Case 2 is poor, and in Cases 4 and 5, because of its poor shadow dispersal capability, it yields a 20.41% and 13.81% reduction in GMP, respectively, exhibiting substantially unsatisfactory performance. As shown in Figure 8, the effectiveness of approaches such as SP, FT, OPS, ST, NO, SK, IS, LP, OEP, MS, CS, AS, and CAM is approximately equal to each other and lower than that of the proposed PT. Furthermore, the current NC, DA, and HEM improve the GMP by almost 26.8%. Besides, the GMP augmentation is limited to only 17.8% because of the ODE's arbitrary reconfiguration and inadequate shade dispersal, which is the least of all. It is evident from the array characteristics shown in Figure 7 that the proposed PT improves the characteristics considerably by significantly mitigating the MPPs.

Because of its uniform shade dispersing ability, the proposed PT approach yielded the highest GMP in Case 2, increasing the GMP by 12.51%. Following PT, the existing OPS and IS both perform better. The SP, FT, NO, SK, LP, CS, and AS strategies improve the GMP by about 10%, whereas the ODE, DA, and SPP approaches only improve it by about 3.98%. Even when compared to standard TCT, the number-based OEP method produces 1.51% less GMP.

Once again, the proposed approach achieves the greatest GMP under Case 3 shading. The GMP yielded by PT is 10,572 W (from Table 3), which is 12.51% greater. The existing SPP, FT, and OS techniques generate 10,553, 10,551, and 10,527 W, respectively, under this case. Other approaches, such as DA and MS, show only a minor increase in GMP. Both ODE and OEP techniques yield the least satisfactory outcomes, resulting in a reduction in output. Except for where they are in the array, the shading patterns in Cases 2 and 3 are identical. The proposed PT results in the same

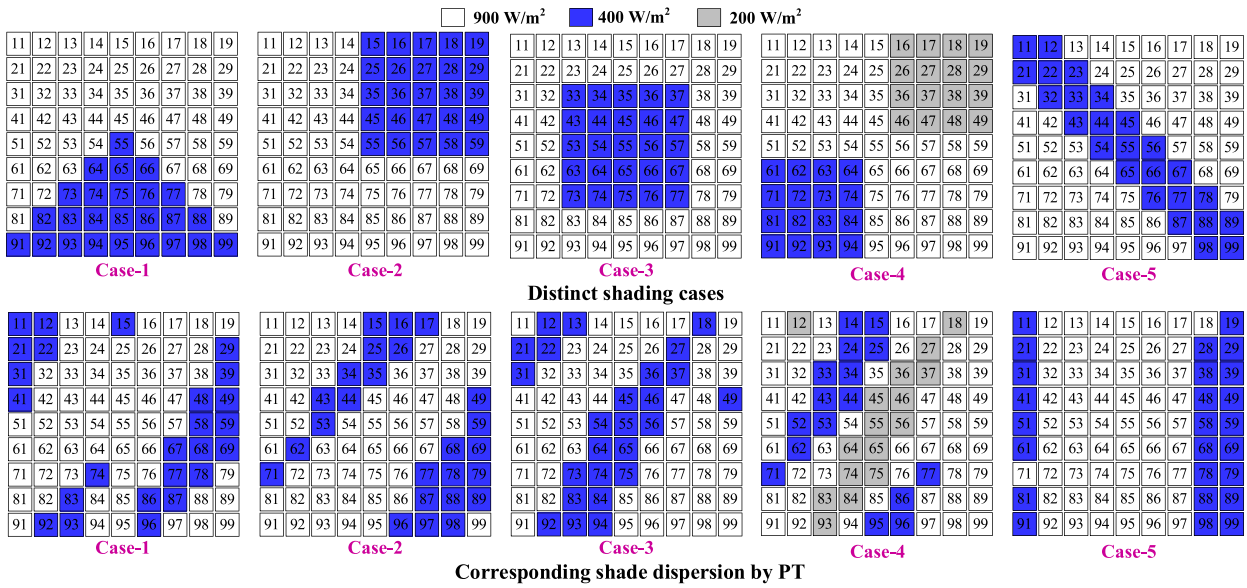

FIGURE 6 Distinct shading cases and the respective shade dispersion by PT approach. PT, Padovan transform. [Colour figure can be viewed at wileyonlinelibrary.com]

TABLE 3 Global maximum power obtained (in watt) by various configurations under Cases 1–5.

Technique	Case 1	Case 2	Case 3	Case 4	Case 5
TCT	7701.5	9393.7	9393.7	8823.5	10,571
SP[18]	10,259	10,350	10,271	8014.2	9782.8
FT[19]	10,259	10,350	10,551	8014.3	10,175
ST[20]	10,334	10,167	10,143	8451.5	9690.1
NC[21]	9661.5	10,257	10,197	7725.2	9571.3
OPS[22]	10,350	10,551	10,257	9271.4	9677.6
NO[22]	10,335	10,342	10,350	8575.1	10,271
IS[24]	10,245	10,511	10,350	8941.6	9250.3
SK[25]	10,347	10,350	10,350	8675.1	9808.8
LP[26]	10,340	10,341	10,271	8682.7	10,549
DA[27]	9764.2	9767.4	9767.2	6871.8	8411.3
ODE[29]	9071.1	9787.7	9333.2	6425.9	9641.5
OS[30]	10,552	10,347	10,527	8671.2	10,123
OEP[31]	10,197	9251.6	9171.9	8673.9	9773.3
MS[33]	10,347	10,350	9761.0	8957.6	9808.6
CS[33]	10,293	10,350	10,267	8018.1	9711.6
AS[34]	10,210	10,345	10,267	8949.8	10,350
HEM[35]	9767.2	9393.9	9393.9	8823.5	10,571
SPP[36]	10,374	9767.2	10,553	7023.5	9095.8
CAM[38]	10,146	10,146	10,145	8451.5	10,571
Proposed PT	10,356	10,572	10,572	9274.4	10,571

(and highest) output power, increasing the GMP by 12.50%, as seen in the results of these two shading cases (2 and 3) in Figure 8. This is because the proposed PT maintains homogeneity by spreading the shade of adjoining panels and ensuring that they are all evenly distributed. The shadow is equally diffused throughout the entire array as a result of its intelligence in maintaining uniformity when reconfiguring panels in the array, ensuring consistent performance regardless of the location of shading. On the contrary, as shown in Figure 8, all existing approaches produce different results for the very same shadowing pattern (when it occurs at a different location), resulting in inconsistent performance. For example, in Case 2, MS generates a 10.17% augmentation, but in Case 3, it only yields an augmentation of 3.8%. The SPP technique, which yields a 12.34% improvement in Case 3, only gains 3.9% in Case 2. In addition, the ODE, which yielded a 4.2% improvement in Case 2, now reduces the GMP by 0.65% in Case 3. The existing indiscriminate reconfiguration procedures of the array are the main reason for this inconsistency in performance. Therefore, the intelligence involved in the proposed methodology proved to be a consistent and efficient solution for reconfiguring the array to distribute the shade evenly.

In Case 4, two edges of the array are considered to be experiencing shadowing of two distinct irradiation levels. The proposed PT approach disperses the shade intelligently while minimizing current variations across the PV array's different rows improving the GMP by 5.06%. Furthermore, the IS, AS, and MS provide sub-optimal performance, with only a 1.35% improvement. Furthermore, all other existing approaches such as SP, FT, ST, NC, NO, SK, LP, OS, ODE, OEP, DA, CS, CAM, and SPP perform poorly even when compared to the benchmark TCT because of their indiscriminate shade dispersion.

In Case 5, the diagonal shading condition that limits the irradiation of an array's diagonal panels is examined. The diagonal shading is very prevalent in the reality; yet, it has not been adequately examined in prior reconfiguration research investigations. Only the proposed PT, as well as the present LP, CAM, and HEM approaches, provides optimal shade dispersal in this scenario. In contrast, all other existing approaches, especially when compared to traditional TCT, provide much lower GMP, as shown in Table 3 and Figure 8. As a result, the arbitrary reconfiguration of the

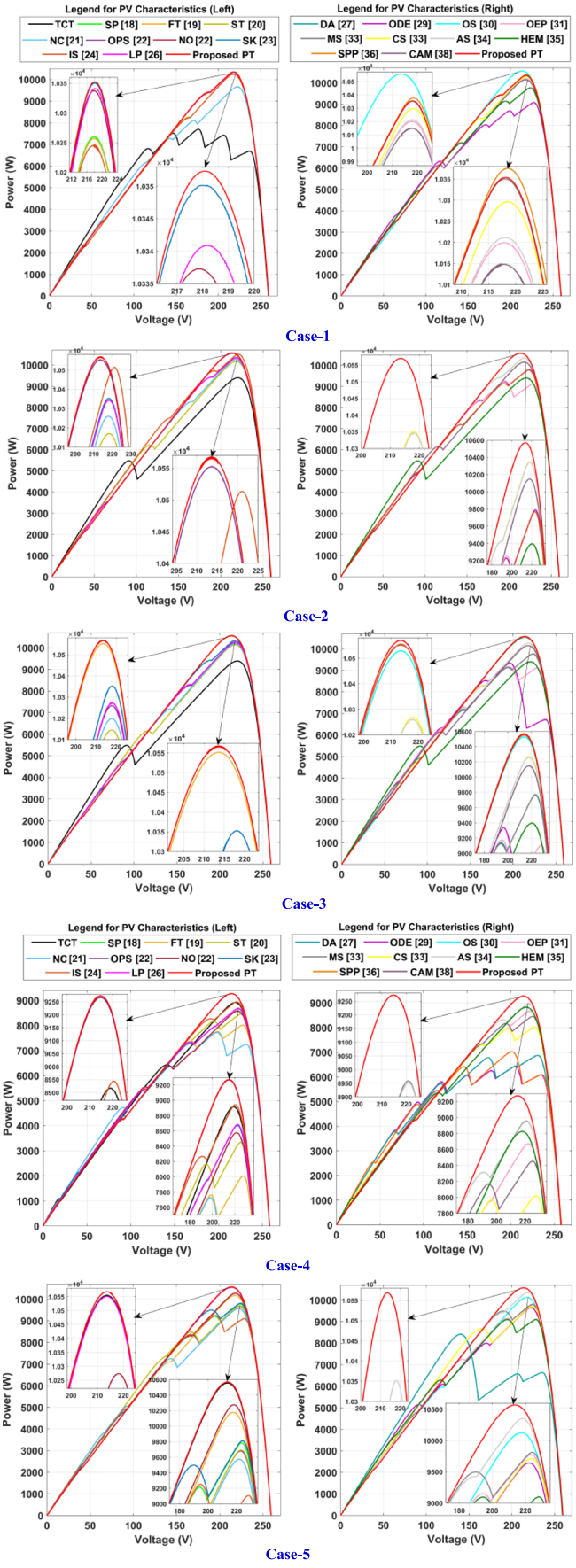

FIGURE 7 Power–voltage characteristics of 9 × 9 array under Cases 1–5. [Colour figure can be viewed at wileyonlinelibrary.com]

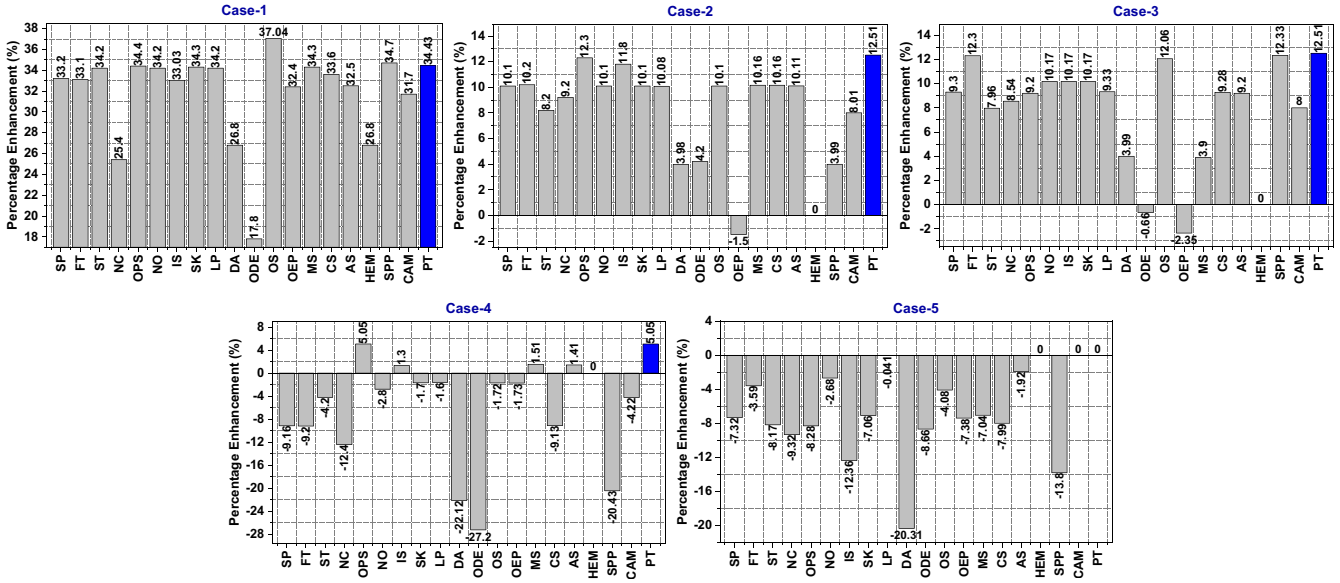

FIGURE 8 Percentage enhancement of GMP of various configurations of 9 × 9 array compared to TCT configuration. GMP, global maximum power. [Colour figure can be viewed at wileyonlinelibrary.com]

existing techniques results in a substantial loss of power rather than a gain. In addition to the existing mismatch losses, indiscriminate shade dispersion causes more additional losses. The ideal reconfiguration method is one that consistently produces improved performance regardless of partially shaded conditions. The proposed PT approach demonstrated its ability to consistently deliver superior results. Figure 7 shows that the array characteristics achieved via PT are greatly improved, with very few MPPs. As a result, using PT simplifies the operation of tracking the GMP by the MPPT controllers. Furthermore, the suggested PT technique exhibits a narrow variation in row currents (as shown in Figure 9) when compared to the existing approaches that greatly reduces mismatch losses. It is also noted from Figure 9 that the existing CAM performs better in exhibiting moderate row current variation compared to TCT; however, it exhibits numerous power peaks which is a major drawback. Similarly, all the existing techniques exhibit many power peaks. When compared to the existing ones, the proposed PT exhibits enhanced characteristics with fewer peaks because of its balanced shade dispersion and hence is proved to be the best solution for shading related issues.

Table 4 demonstrates the effect of implementing the proposed PT strategy on mitigating the difference of irradiation of PV array rows before and after the reconfiguration. After the reconfiguration, the range between the minimum and maximum sum of row irradiations significantly narrows compared to the initial range before array adjustment. This reduction highlights an improvement in array characteristics and a decrease in mismatch losses.

4.2 | Scalability and effectiveness of proposed strategy for asymmetric arrays

Because most of the present static reconfiguration strategies are developed on logic-based, puzzle-based, and magic square-based procedures that are only applicable to symmetric grids,[46–50] they are incompatible with asymmetric arrays. However, the solar PV arrays can indeed be symmetric or asymmetric in practicality. The number-based ODE[29] and OEP,[31] as well as the chaotic-based HEM[35] approaches, have recently been proposed to overcome this disadvantage of the aforementioned techniques. The OE, OEP, and HEM approaches, despite being functional with asymmetric arrays, have poor shade dispersion. A 4 × 8 array is studied and evaluated under eight different circumstances to validate the efficiency of the suggested PT approach for asymmetric arrays, as shown in Figure 10. Their performance was also compared to that of the more recent ODE[29] and OEP[31] approaches.

The proposed strategy, as shown in Figure 10, exhibits even shade distribution, resulting in fewer MPPs (power peaks) and improved the PV characteristics greatly, as demonstrated in Figure 11. Unlike the existing configurations, the PV characteristics obtained by the proposed PT are smoother having only one or two peaks making the GMP tracking quite easier for the MPPT controllers. In consequence, the cost and complexity of the MPPT controller necessitated

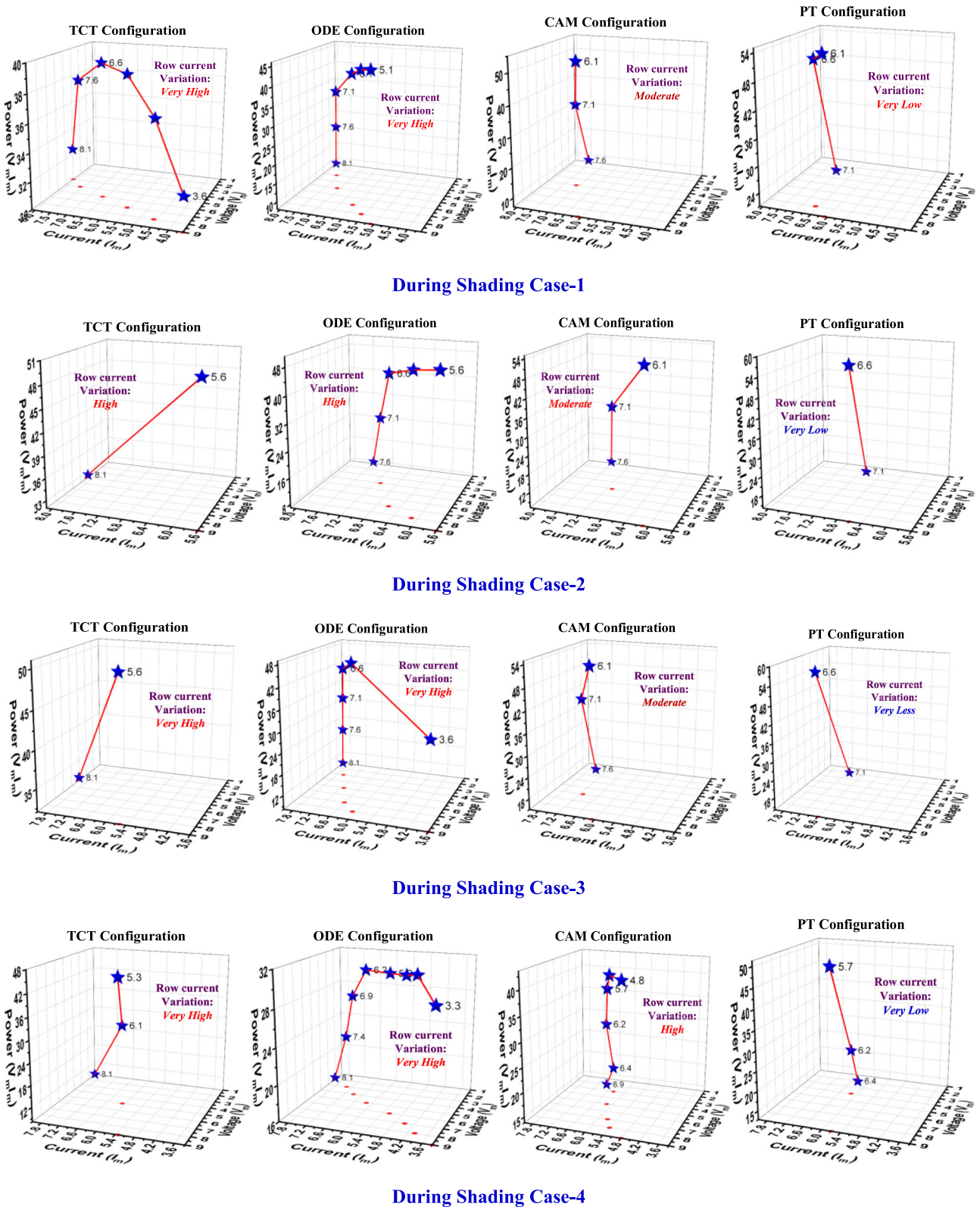

FIGURE 9 Row current variation and number of MPPs of various configurations of 9 × 9 array. MPPs, multiple power peaks. [Colour figure can be viewed at wileyonlinelibrary.com]

is significantly reduced. The proposed PT also has the highest GMP in all shading circumstances because of its superior shade dispersion. As a result, it is worth noting that the proposed FT approach is both compatible and efficacious in partial shading scenarios.

TABLE 4 Row irradiation of PV array for 9 × 9 array before and after the implementation of the proposed PT strategy.

	Row irradiation (W/m^2)				
Shading case	**Range**	**Before reconfiguration**	**Difference**	**After reconfiguration**	**Difference**
Case 1	Min	3600	4500	6600	500
	Max	8100		7100	
Case 2	Min	5600	2500	6600	500
	Max	8100		7100	
Case 3	Min	5600	2500	6600	500
	Max	8100		7100	
Case 4	Min	5300	2800	5600	800
	Max	8100		6400	
Case 5	Min	6600	500	6600	500
	Max	7100		7100	

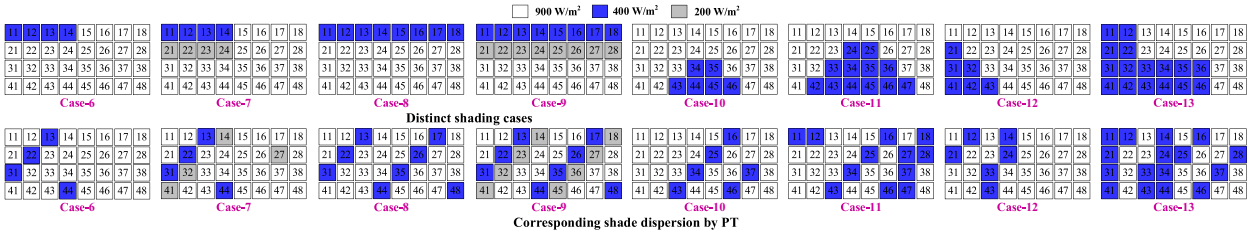

FIGURE 10 Distinct shading cases and the respective shade dispersion by PT approach. PT, Padovan transform. [Colour figure can be viewed at wileyonlinelibrary.com]

4.3 | Experimental validation of proposed strategy

The proposed reconfiguration mechanism for a 4 × 4 PV array is shown in Figure 12 by a laboratory experimental prototype that has been created. The experimental test bench is made up of sixteen 3-W solar panels, a source of artificial lighting made up of numerous double-ended halogen light bulbs with a knob to control intensity, a load that is a (300, 1.5 A) variable sliding rheostat, plug connectors to reconfigure the array in different configurations, and transparent sheets to limit the irradiation to simulate various artificial shading conditions. To measure the respective PV array current and voltage, two multimeters were connected in series and parallel to the array. With the proper arrangement of halogen bulbs over the PV panels, homogeneous irradiation levels are maintained over all of the panels. Each halogen lamp typically produces up to 400 W/m^2 of irradiation. A portable solar power meter and an infrared temperature gun are used to measure the incident irradiance and operational temperature of the panels. Each module of the prototype model has positive and negative tapings, enabling it to be reconfigured using banana connections in distinct configurations. The array output terminals are connected to a variable rheostat that would be adjusted to harvest maximum power from different array configurations. Because the proposed configuration is static, no extra electrical or electronic equipment/devices are required for hardware execution. This eliminates the need for sensors, switches, and other costly equipment. The designed 4 × 4 array generates 17.2 W under normal unshaded operation conditions, with incoming irradiation from artificial illumination source estimated to be roughly 330 W/m^2 and an operating temperature of around 29°C. The 4 × 4 PV modules are configured in TCT, LAS,[23] MGS,[28] DIT,[30] and PT topologies and evaluated under six shading conditions, as illustrated in Figure 13. The irradiation levels for the non-shaded and shaded panels are around 300 and 150 W/m^2, respectively.

Because of its uniform shade dispersion across the array, the proposed PT approach produces the lowest row current mismatch, resulting in the highest output in all shading circumstances. On the contrary, as shown in Figure 14, existing

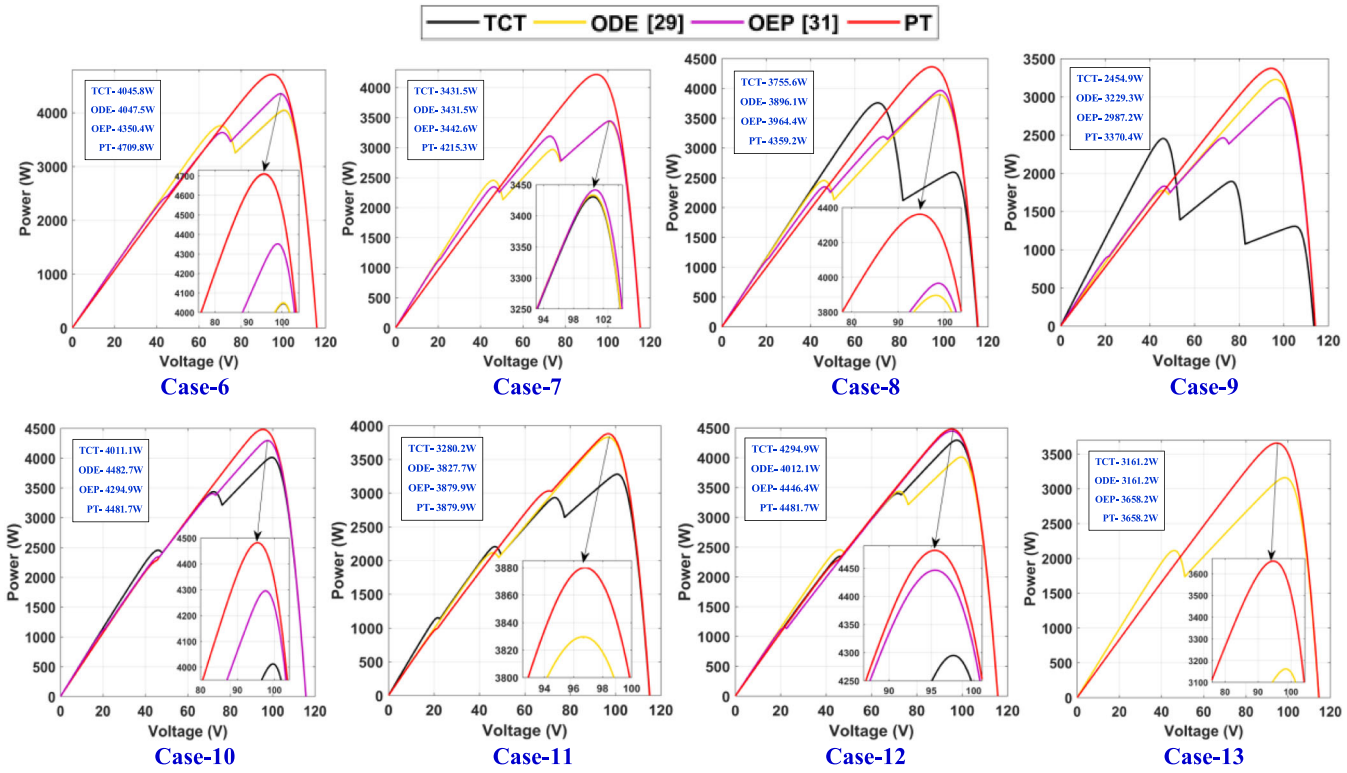

FIGURE 11 Power–voltage characteristics of 4 × 8 asymmetric PV array under Cases 6–13. PV, photovoltaic. [Colour figure can be viewed at wileyonlinelibrary.com]

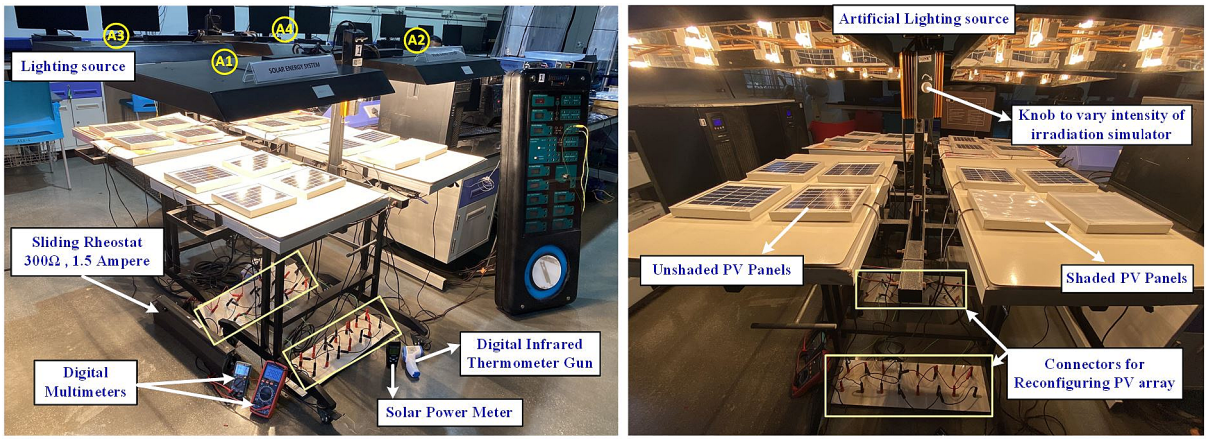

FIGURE 12 Laboratory experimental prototype of the proposed reconfiguration system. [Colour figure can be viewed at wileyonlinelibrary.com]

approaches deliver very unreliable performance. The existing DIT improves the power output just in two cases (Cases 12 and 14), whereas the MGS and LAS topologies enhance power output in three of six conditions. This inconsistency is because of their indiscriminate reconfiguration method, which has resulted in arbitrary shade dispersion. Furthermore, the MGS, LAS, and DIT configurations fail in diagonally shading cases 18 and 19 as a result, even when compared to normal TCT, the output is the lowest. However, as demonstrated in Figure 14, the proposed PT strategy maintains its consistency in producing superior performance in all scenarios (because of its intelligent shadow dispersion). The power–voltage characteristics of a 4 × 4 PV array under Cases 14–19 are shown in Figure 15.

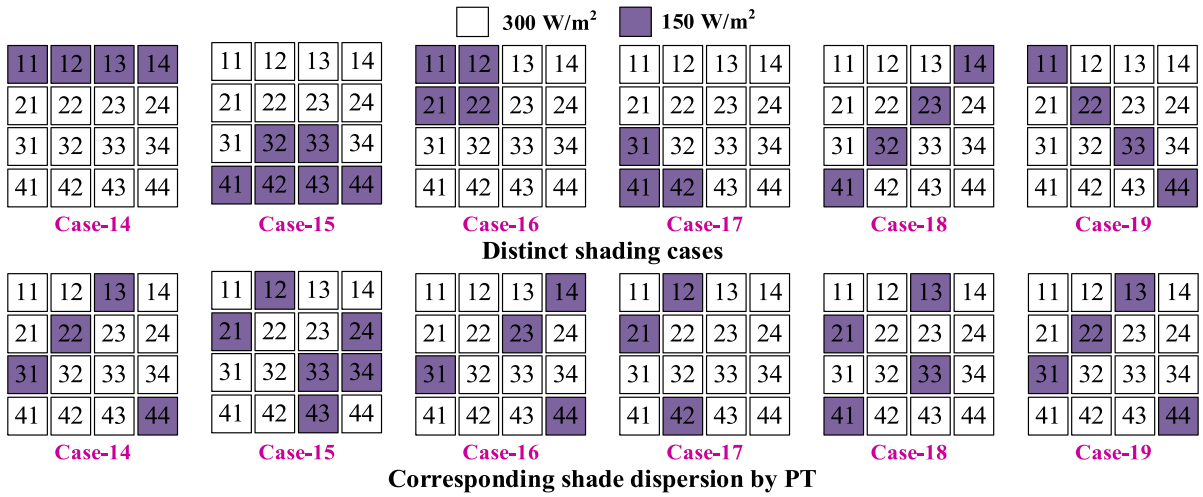

FIGURE 13 Distinct shading cases and corresponding shading obtained by PT-based topology. PT, Padovan transform. [Colour figure can be viewed at wileyonlinelibrary.com]

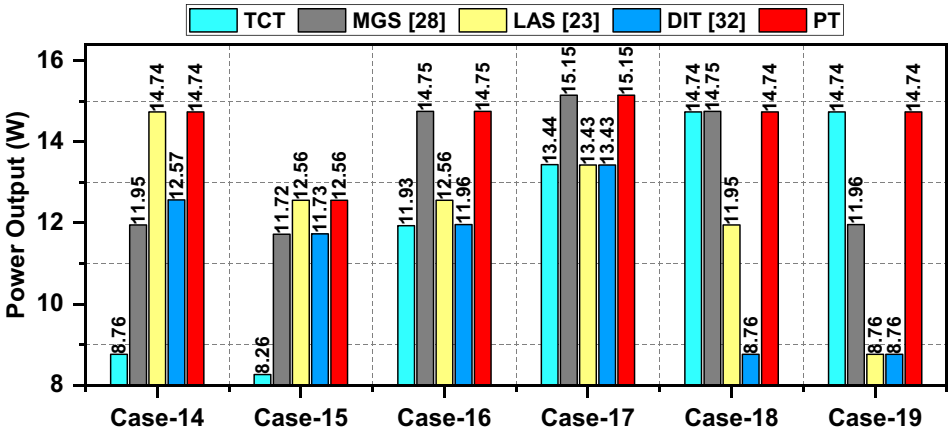

FIGURE 14 Experimental values of power output of various configurations under distinct shading cases. [Colour figure can be viewed at wileyonlinelibrary.com]

4.4 | Experimental validation of reconfiguration strategy with MPPT controller

The effectiveness of the proposed reconfiguration methodology for the PV array and its advantages has been demonstrated by validating it with the conventional MPPT controller. The widely used INC-based MPPT control has been employed to track the GMP. The laboratory experimental setup for the real-time validation is shown in Figure 16. For emulating the solar irradiation, the Chroma 62100H-600S solar PV emulator has been used. The solar emulator works with the supply voltage of 400 V as supply and hence a three-phase auto transformer is used to set up the required voltage to the emulator. The required array characteristics are loaded in the PV emulator using the excel file containing the voltages and currents of the array. A DC–DC boost converter connected to a resistive load is supplied from the emulator. The array's voltage and current from the PV emulator is sensed using the voltage sensor (LV-25P) and current sensor (LA-25P) and is given to the dSPACE controller. The conventional INC-based MPPT algorithm (described in Section 3) has been dumped in the dSPACE controller. Based on the sensed data of voltage and current, the dSPACE controller generates pulses to the MOSFET of the converter through the gate driver circuit board as shown in Figure 17. The employed sensors and driver board is powered with 15-V AC supply. The linkage between the test bench components and devices of the overall experimental setup is shown in Figure 17. The resistive load is kept constant throughout the procedure, and the tracking of GMP by the INC MPPT controller for various varying shading conditions is observed and studied. The specifications of overall PV system used in experimentation is shown in Table A3.

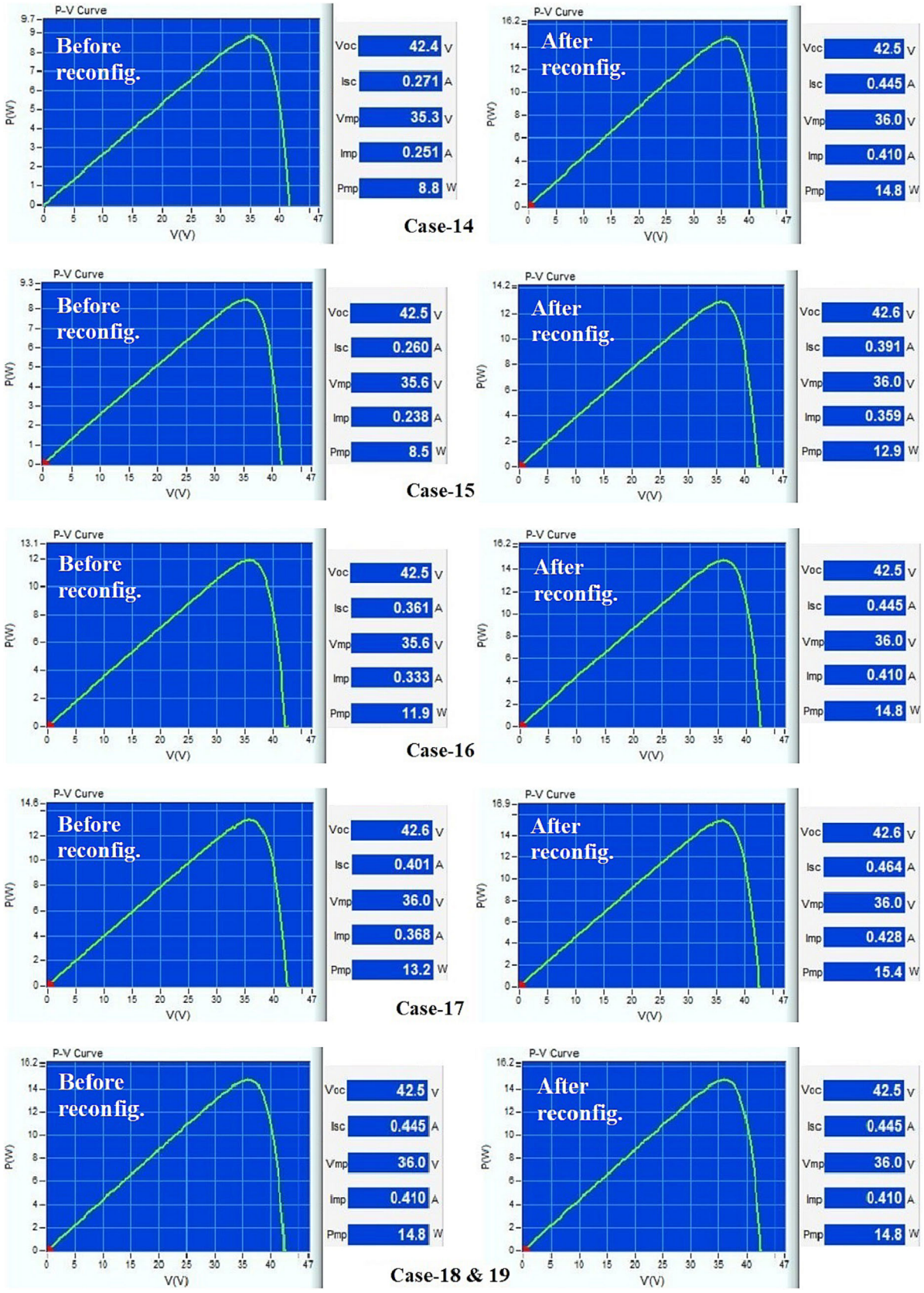

FIGURE 15 Power–voltage characteristics of a 4 × 4 asymmetric array under Cases 14–19. [Colour figure can be viewed at wileyonlinelibrary.com]

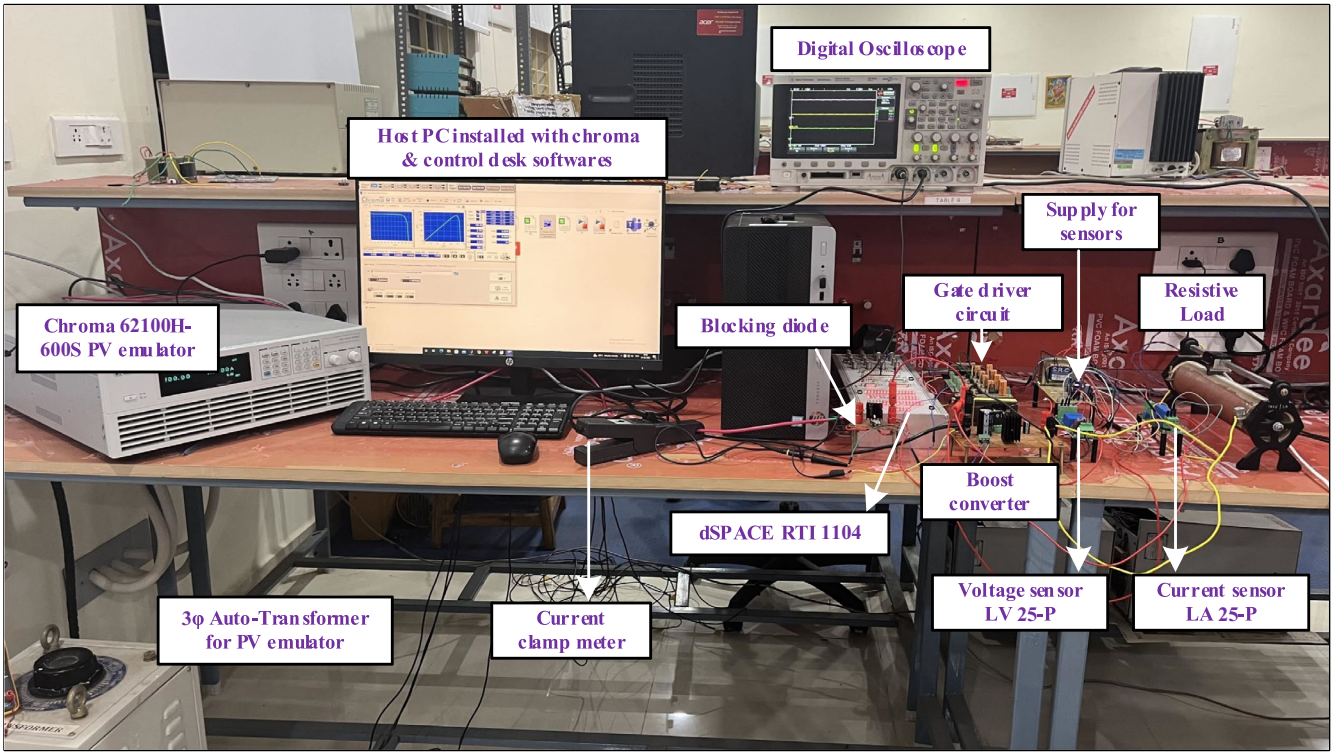

FIGURE 16 Laboratory experimental setup for the real-time validation using MPPT control. MPPT, maximum power point tracking. [Colour figure can be viewed at wileyonlinelibrary.com]

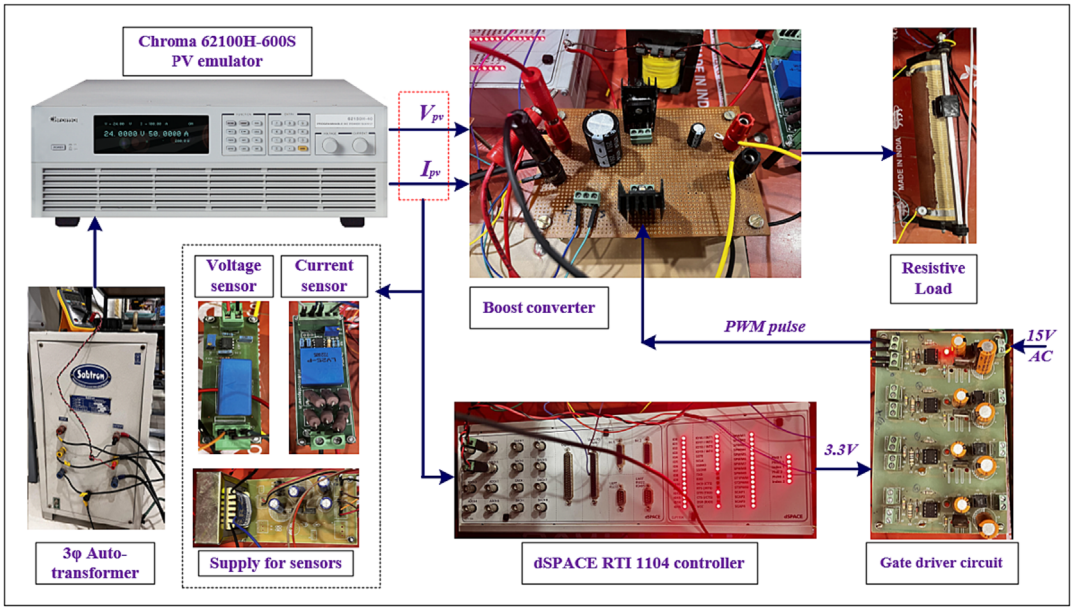

FIGURE 17 Linkage between the test bench components and devices. [Colour figure can be viewed at wileyonlinelibrary.com]

The proposed reconfiguration methodology has been implemented for the PV array and tested under the shading cases shown in Figure 18. Generally in some cases, the conventional MPPT control algorithms like INC and P & O fails to tracks the GMP effectively. Because of their inherit limitations, they stuck at the local maxima failing to track the GMP. This is reflected in the experimental results as shown in Figures 21 and 22. Before reconfiguration, the MPPT controller tracks the GMP of 197.1 W in Case 20 effectively (Figure 19), whereas after reconfiguration, the local peaks

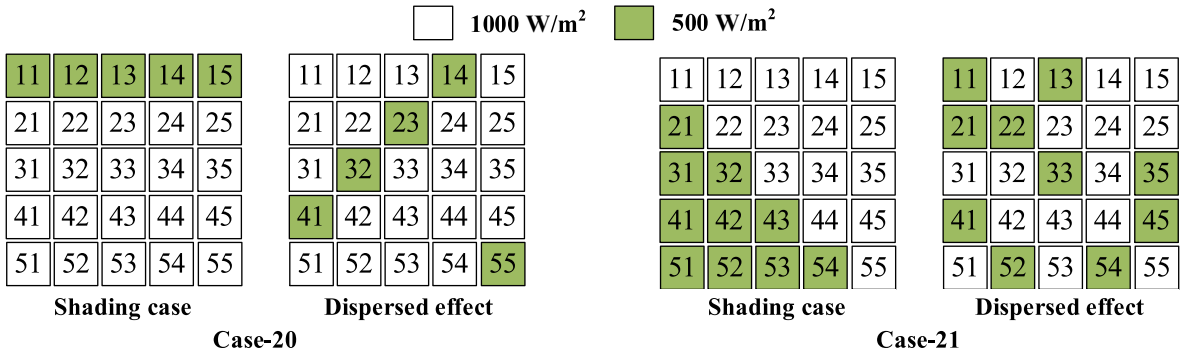

FIGURE 18 Shading cases (20 and 21) and corresponding shading obtained by PT-based topology. PT, Padovan transform. [Colour figure can be viewed at wileyonlinelibrary.com]

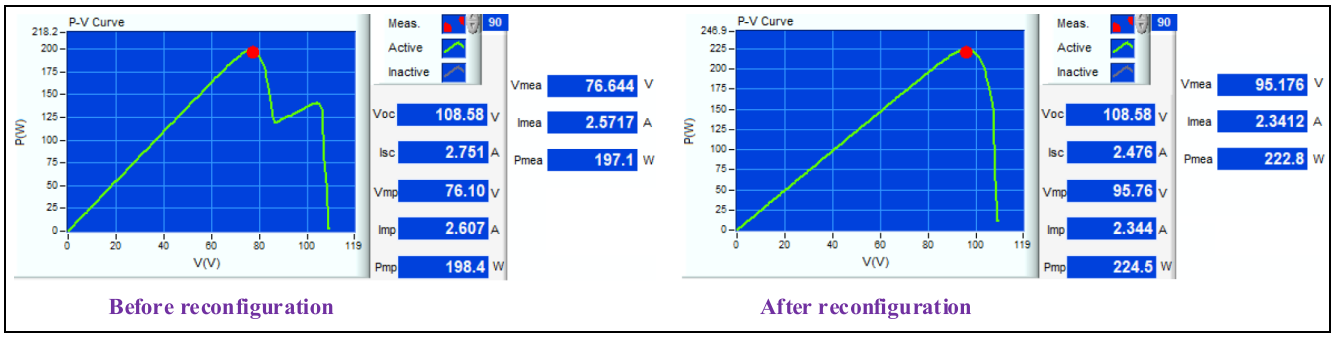

FIGURE 19 Power–voltage characteristics under Case 20 shading. [Colour figure can be viewed at wileyonlinelibrary.com]

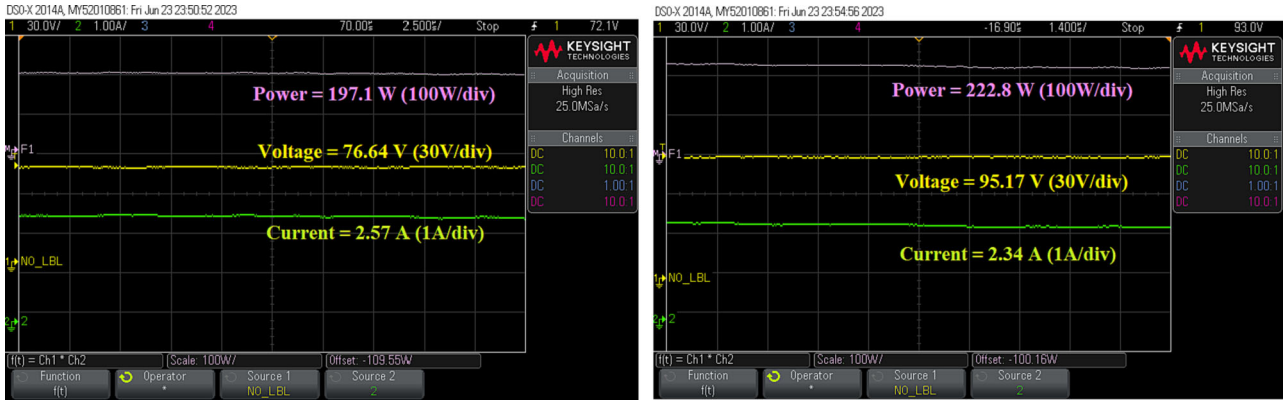

FIGURE 20 GMP tracked by the INC MPPT controller before reconfiguration (left) and after (right) reconfiguration under Case 20. GMP, global maximum power; INC, incremental conductance; MPPT, maximum power point tracking. [Colour figure can be viewed at wileyonlinelibrary.com]

are eliminated and further the GMP value is also enhanced to 222.8 W which is a significant increment (Figure 20). In Case 21 shading, the PV array exhibits five multiple power peaks (Figure 21), out of which the conventional MPPT controller gets trapped in the local maxima thereby yielding only 136.5 W (Figure 22). The actual GMP that has to be tracked by the MPPT controller is 163.6 W. However, upon implementing the proposed algorithm, all the multiple peaks have been eliminated because of the uniformly dispersed shading, and in consequence, the GMP is also significantly enhanced to 197.2 W.

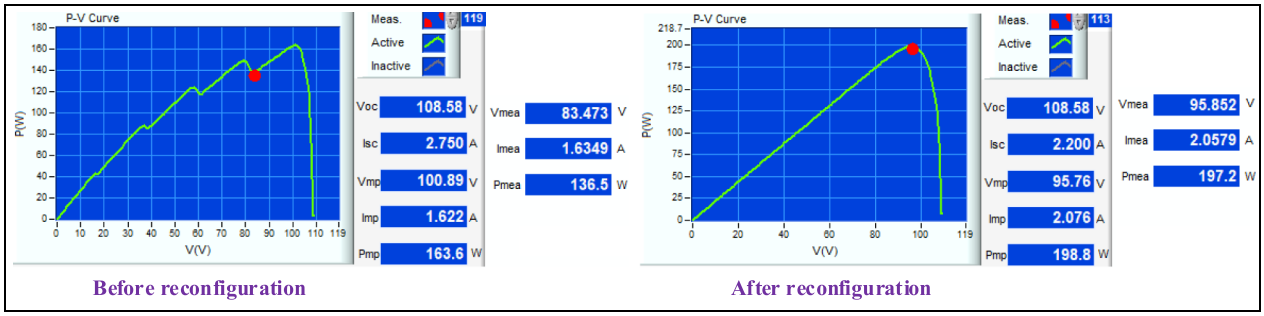

FIGURE 21 Power–voltage characteristics under Case 21 shading. [Colour figure can be viewed at wileyonlinelibrary.com]

FIGURE 22 GMP tracked by the INC MPPT controller before reconfiguration (left) and after (right) reconfiguration under Case 21. GMP, global maximum power; INC, incremental conductance; MPPT, maximum power point tracking. [Colour figure can be viewed at wileyonlinelibrary.com]

TABLE 5 Values of $R+$, $R-$, and p-value for various configurations.

PT vs	R_+	R_-	p-value	PT vs	R_+	R_-	p-value
TCT	10	0	0.067889	DA[27]	15	0	0.043113
SP[18]	15	0	0.043113	ODE[29]	15	0	0.043113
FT[19]	15	0	0.043113	OS[30]	10	0	0.067889
ST[20]	15	0	0.043113	OEP[31]	15	0	0.043113
NC[21]	15	0	0.043113	DIT[32]	21	0	0.027707
OSA[22]	15	0	0.043113	MS[33]	15	0	0.043113
NO[22]	15	0	0.043113	CS[33]	15	0	0.043113
LAS[23]	10	0	0.067889	AS[34]	15	0	0.043113
IS[24]	15	0	0.043114	HEM[35]	10	0	0.067889
SK[25]	10	0	0.067889	SPA[36]	10	0	0.067889
LP[26]	10	0	0.067889	CAM[38]	10	0	0.067889

5 | EVALUATION OF OVERALL PERFORMANCE USING THE WILCOXON SIGNED-RANK TEST

A pairing-wise independent comparison study of the evaluated procedures, as shown in Table 5, was conducted using a nonparametric statistical hypothesis Wilcoxon signed-rank sum test[51] with a statistically significant difference, p-value of 0.05 to determine the reliability and consistency in performance by PT approach under various shade situations and

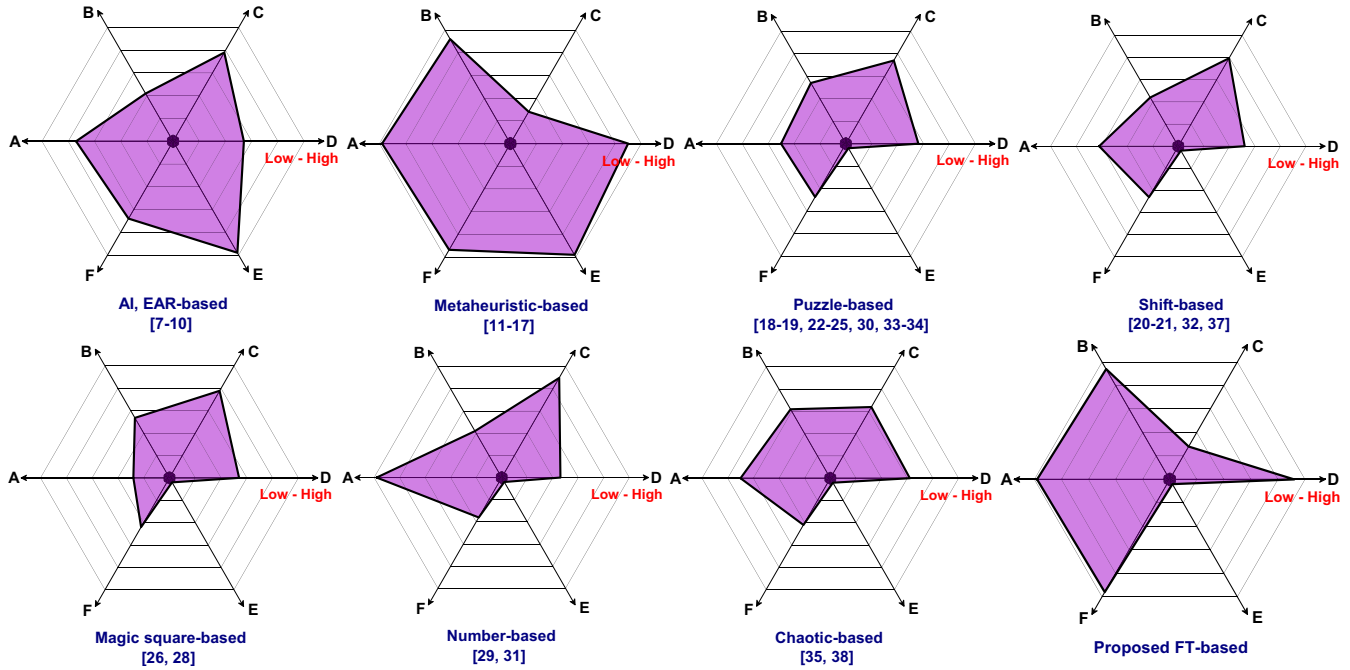

FIGURE 23 Radar charts showing the comparison of overall performance of existing reconfiguration approaches with the existing ones. GMP, global maximum power. MPPs, multiple power peaks. [Colour figure can be viewed at wileyonlinelibrary.com]

to quantitatively highlight its notable deviation compared to previous techniques. The below procedure is followed to carry out the test.

1. Determine the GMP for various solar array configurations in different partial shading scenarios.
2. Calculate "$R+$," the sum of positive ranks for which the proposed technique outperforms the previous ones in terms of GMP.
3. Find the value of "$R-$," the sum of negative rankings for which current methods provide higher GMP compared with the proposed approach.
4. In a statistical hypothesis test, calculate a p-value that indicates the significant variation of the collected results. The lower the p-value (0.05), the more evidence there is against the null hypothesis, implying a significant difference between the methodologies.

The p-values for 14 approaches are less than 0.05 (as shown in Table 5), indicating that there is a significant difference between the proposed PT and the existing techniques. Furthermore, the p-values for the remaining eight approaches are 0.067 (slightly higher than 0.05), implying that there is still a substantial difference in their performances. Because $R+$ is significantly greater than $R-$, the evaluated $R+$, $R-$, and p values suggest that the proposed PT is competent of obtaining the largest GMP than the existing ones. Furthermore, the proposed technique demonstrates its superiority in delivering an effectively constant performance for various array sizes under all shading situations. The radar charts shown in Figure 23 shows the comparison of overall performance of existing reconfiguration approaches with the proposed PT.

6 | CONCLUSIONS

A comprehensive literature review of existing reconfiguration approaches is presented, along with their pros and cons. To reduce shading losses efficiently, a distinctive reconfiguration strategy motivated by the number sequence-based PT while adopting the principle of image processing is suggested. The proposed PT approach overcomes the shortcomings of the existing strategies to a larger degree. Further, it is tested for symmetrical and asymmetric PV arrays during 21 shading scenarios, and its efficacy is compared to the 23 existing static reconfiguration strategies. The GMP enhancement with the proposed PT configuration for 9×9 and 4×8 PV arrays is in the range of (5.06–34.43)% and (4.34–

37.40)%, respectively. The PT approach is unique in that it evenly distributes shade by minimizing the row current mismatch by decreasing the correlation between neighboring shaded modules of an array. This distinguishing feature obtained the highest GMP with better characteristics only with fewest MPPs, alleviating the stress on MPPT controllers. The proposed reconfiguration strategy integrated with MPPT is validated experimentally using a prototype model. Additionally, the statistical Wilcoxon signed-rank sum analysis with the lowest *p*-value shows that the proposed method is more consistent and efficient than the ones currently in use. The proposed PT-based encryption strategy for reconfiguration offers the best solution for significantly reducing shading impact with the enhanced array characteristics, based on the comprehensive qualitative and quantitative study.

CONFLICT OF INTEREST STATEMENT

No potential competing interest was reported by the authors.

DATA AVAILABILITY STATEMENT

Data sharing is not applicable to this article as no new data were created or analyzed in this study.

ORCID

Rayappa David Amar Raj https://orcid.org/0000-0002-5888-5513
Thanikanti Sudhakar Babu https://orcid.org/0000-0003-0737-3961

REFERENCES

1. Raj RDA, Naik KA. A novel scan pattern for reconfiguration of partially shaded photovoltaic arrays for maximum power extraction. *Int J Circuit Theory Applic*. 2022;51(2):668-701. doi:10.1002/cta.3452
2. Aljafari B, Satpathy PR, Thanikanti SB. Partial shading mitigation in PV arrays through dragonfly algorithm based dynamic reconfiguration. *Energy*. 2022;257:124795, ISSN 0360-5442. doi:10.1016/j.energy.2022.124795
3. Raj et al. A novel solar photovoltaic array reconfiguration technique using two-dimensional generalized Arnold's cat map. *ASME J sol Energy Eng*. 2022;144(6):061001. doi:10.1115/1.4054506
4. Ali AIM, Ramadan H, Mohamed A. Improved P&O MPPT algorithm with efficient open-circuit voltage estimation for two-stage grid-integrated PV system under realistic solar radiation. *Int J Electrical Power Energy Syst*. 2022;137:107805. doi:10.1016/j.ijepes.2021.107805
5. Nassef AM, Houssein EH, Helmy BE, Rezk H. Modified honey badger algorithm based global MPPT for triple-junction solar photovoltaic system under partial shading condition and global optimization. *Energy*. 2022;124363, ISSN 0360-5442. doi:10.1016/j.energy.2022.124363
6. Sousa SM, Gusman LS, Lopes TAS, Pereira HA, Callegari JMS. MPPT algorithm in single loop current-mode control applied to dc–dc converters with input current source characteristics. *Int J Electrical Power Energy Syst*. 2022;138:107909. doi:10.1016/j.ijepes.2021.107909
7. Velasco-Quesada G, Guinjoan-Gispert F, Pique-Lopez R, Roman-Lumbreras M, Conesa-Roca A. Electrical PV array reconfiguration strategy for energy extraction improvement in grid-connected PV systems. *IEEE Trans Ind Electron*. 2009;56(11):4319-4331. doi:10.1109/TIE.2009.2024664
8. Varma GHK, Barry VR, Jain RK. A total-cross-tied-based dynamic photovoltaic array reconfiguration for water pumping system. *IEEE Access*. 2022;10:4832-4843. doi:10.1109/ACCESS.2022.3141421
9. Karakose M, Baygin M, Murat K, Baygin N, Akin E. Fuzzy based reconfiguration method using intelligent partial shadow detection in PV arrays. *Int J Comput Intell Syst*. 2016;9(2):202-212. doi:10.1080/18756891.2016.1150004
10. Karakose M, Baygin M, Murat K, Baygin N, Akin E. Fuzzy based reconfiguration method using intelligent partial shadow detection in PV arrays. *Intl J Comput Intell Syst*. 9(2):202-212.
11. Deshkar SN, Dhale SB, Mukherjee JS, Babu TS, Rajasekar N. Solar PV array reconfiguration under partial shading conditions for maximum power extraction using genetic algorithm. *Renew Sustain Energy Rev*. 2015;43:102-110. doi:10.1016/j.rser.2014.10.098
12. Babu TS, Ram JP, Dragičević T, Miyatake M, Blaabjerg F, Rajasekar N. Particle swarm optimization based solar PV array reconfiguration of the maximum power extraction under partial shading conditions. *IEEE Trans Sustain Energy*. 2018;9(1):74-85. doi:10.1109/TSTE.2017.2714905
13. Fathy A. Butterfly optimization algorithm based methodology for enhancing the shaded photovoltaic array extracted power via reconfiguration process. *Energ Conver Manage*. 2020;220:113115. doi:10.1016/j.enconman.2020.113115
14. Yousri D, Thanikanti SB, Balasubramanian K, Osama A, Fathy A. Multi-objective grey wolf optimizer for optimal design of switching matrix for shaded PV array dynamic reconfiguration. *IEEE Access*. 2020;8:159931-159946. doi:10.1109/ACCESS.2020.3018722
15. Fathy A. Recent meta-heuristic grasshopper optimization algorithm for optimal reconfiguration of partially shaded PV array. *Solar Energy*. 2018;171:638-651, ISSN 0038-092X. doi:10.1016/j.solener.2018.07.014
16. Ajmal AM, Ramachandaramurthy VK, Naderipour A, Ekanayake JB. Comparative analysis of two-step GA-based PV array reconfiguration technique and other reconfiguration techniques. *Energy Conv Manag*. 2021;230:113806. doi:10.1016/j.enconman.2020.113806
17. Yousri D, Babu TS, Mirjalili S, Rajasekar N, Elaziz MA. A novel objective function with artificial ecosystem-based optimization for relieving the mismatching power loss of large-scale photovoltaic array. *Energ Conver Manage*. 2020;225:113385. doi:10.1016/j.enconman.2020.113385

18. Rani BI, Ilango GS, Nagamani C. Enhanced power generation from PV array under partial shading conditions by shade dispersion using Su do Ku configuration. *IEEE Trans Sustain Energy*. 2013;4(3):594-601. doi:10.1109/TSTE.2012.2230033
19. Sahu HS, Nayak SK, Mishra S. Maximizing the power generation of a partially shaded PV array. *IEEE J Emerging Selected Top Power Electron*. 2016;4(2):626-637.
20. Belhaouas N, Ait Cheikh M-S, Agathoklis P, et al. PV array power output maximization under partial shading using new shifted PV array arrangements. *Appl Energy*. 2017;187:326-337. doi:10.1016/j.apenergy.2016.11.038
21. Pillai DS, Ram JP, Nihanth MSS, Rajasekar N. A simple, sensorless and fixed reconfiguration scheme for maximum power enhancement in PV systems. *Energy Conv Manag*. 2018;172:402-417. doi:10.1016/j.enconman.2018.07.016
22. Horoufiany M, Ghandehari R. Optimization of the Sudoku based reconfiguration technique for PV arrays power enhancement under mutual shading conditions. *Sol Energy*. 2018;159:1037-1046. doi:10.1016/j.solener.2017.05.059
23. Pachauri R, Yadav AS, Chauhan YK, Sharma A, Kumar V. Shade dispersion-based photovoltaic array configurations for performance enhancement under partial shading conditions. *Int Trans Electr Energy Syst*. 2018;28(7):e2556. doi:10.1002/etep.2556
24. Krishna S, Moger T. Improved SuDoKu reconfiguration technique for total-cross-tied PV array to enhance maximum power under partial shading conditions. *Renew Sustain Energy Rev*. 2019;109:333-348. doi:10.1016/j.rser.2019.04.037
25. Nihanth MSS, Ram JP, Pillai DS, Ghias AMYM, Garg A, Rajasekar N. Enhanced power production in PV arrays using a new skyscraper puzzle based one-time reconfiguration procedure under partial shade conditions (PSCs). *Solar Energy*. 2019;194:209-224. doi:10.1016/j.solener.2019.10.020
26. Venkateswari R, Rajasekar N. Power enhancement of PV system via physical array reconfiguration based Lo Shu technique. *Energ Conver Manage*. 2020;215:112885. doi:10.1016/j.enconman.2020.112885
27. Nihanth MSS, Rajasekar N, Pillai DS, Ram JP. A new array reconfiguration scheme for solar PV systems under partial shading conditions. In: *Intelligent Computing Techniques for Smart Energy Systems. Lecture Notes in Electrical Engineering*. Vol.607; 2020.
28. Rakesh N, Madhavaram TV. Performance enhancement of partially shaded solar PV array using novel shade dispersion technique. *Front Energy*. 2016;10(2):227-239. doi:10.1007/s11708-016-0405-y
29. Yadav K, Kumar B, Swaroop D. Mitigation of mismatch power losses of PV array under partial shading condition using novel odd even configuration. *Energy Rep*. 2020;6:427-437. doi:10.1016/j.egyr.2020.01.012
30. Krishna SG, Moger T. Optimal SuDoKu reconfiguration technique for total-cross-tied PV array to increase power output under non-uniform irradiance. *IEEE Trans Energy Convers*. 2019;34(4):1973-1984. doi:10.1109/TEC.2019.2921625
31. Reddy SS, Yammani C. Odd-even-prime pattern for PV array to increase power output under partial shading conditions. *Energy*. 2020;2013:118780. doi:10.1016/j.energy.2020.118780
32. Madhanmohan VP, Nandakumar M, Saleem A. Enhanced performance of partially shaded photovoltaic arrays using diagonally dispersed total cross tied configuration. *Energy Sources, Part a: Recovery Utilization Environ Effects*. 2020;1-19. doi:10.1080/15567036.2020.1826008
33. Anjum S, Mukherjee V, Mehta G. Advanced SuDoKu-based reconfiguration strategies for maximum power extraction from partially shaded solar photovoltaic array. *ASME JSol Energy Eng*. 2021;143(6):061003.
34. Bharti, Tatabhatla VMR, Kanumuri T. Power maximization under partial shading conditions using advanced Sudoku configuration. In: *Proceedings of the International Conf. on Paradigms of Computing, Communication and Data Sciences*. Vol.15; 2021.
35. Raj RDA, Naik KA. A generalized Henon map-based solar PV array reconfiguration technique for power augmentation and mismatch mitigation. *IETE J Res*. 2022. doi:10.1080/03772063.2022.2055660
36. Cherukuri SK, Balachandran PK, Kaniganti KR, et al. Power enhancement in partial shaded photovoltaic system using spiral pattern array configuration scheme. *IEEE Access*. 2021;9:123103-123116. doi:10.1109/ACCESS.2021.3109248
37. Krishnan VR, Blaabjerg F, Sangwongwanich A, Natarajan R. Twisted two-step arrangement for maximum power extraction from a partially shaded PV array. *IEEE J Photovolt*. 2022;12(3):871-879. doi:10.1109/JPHOTOV.2022.3143456
38. Tatabhatla VMR, Agarwal A, Kanumuri T. A chaos map based reconfiguration of solar array to mitigate the effects of partial shading. *IEEE Trans Energy Convers*. 2022;37(2):811-823. doi:10.1109/TEC.2021.3122470.
39. Lomelí ACG, Hernández SH, Luca F. Fibonacci numbers as sums of two Padovan numbers. *Afrika Matematika*. 2022;33(1):14. doi:10.1007/s13370-021-00943-0
40. Anatriello G, Németh L, Vincenzi G. Generalized Pascal's triangles and associated k-Padovan-like sequences. *Math Comput Simul*. 2022;192:278-290, ISSN 0378-4754,. doi:10.1016/j.matcom.2021.09.006
41. Ddamulira M. On the x-coordinates of Pell equations that are sums of two Padovan numbers. *Bol Soc Mat Mex*. 2021;27(1):4. doi:10.1007/s40590-021-00312-8
42. Wang C, Zhang Y. A novel image encryption algorithm with deep neural network. *Signal Process*. 2022;196:108536. doi:10.1016/j.sigpro.2022.108536
43. Mishra M, Mishra P, Adhikary MC, Kumar S. Image encryption using Fibonacci-Lucas transformation. *Int J Cryptogr Information Secur*. 2012;2(3):131-141.
44. Raj RDA, Naik KA. Optimal reconfiguration of PV array based on digital image encryption algorithm: a comprehensive simulation and experimental investigation. *Energ Conver Manage*. 2022;261:115666. doi:10.1016/j.enconman.2022.115666
45. Amar Raj RD, Naik KA. Solar array optimization using cryptographic Fibonacci transformation for global power enhancement and ease of MPPT controllers. *Energ Technol*. 2023;11(9):2300380. doi:10.1002/ente.202300380
46. Satpathy PR et al. An efficient power extraction technique for improved performance and reliability of solar PV arrays during partial shading. *Energy*. 2023;282:128992, ISSN 0360-5442. doi:10.1016/j.energy.2023.128992

47. Mallick P, Sharma R, et al. A dimension-independent array relocation (DIAR) approach for partial shading losses minimization in asymmetrical photovoltaic arrays. *IEEE Access*. 2023;11:63176-63196. doi:10.1109/ACCESS.2023.3288329
48. Aljafari B, et, al. A zero switch and sensorless reconfiguration approach for sustainable operation of roof-top photovoltaic system during partial shading. *IET Renew Power Gener*. 2023;17(6):1385-1412. doi:10.1049/rpg2.12683
49. Satpathy PR, Bhowmik P, Babu TS, Sain C, Sharma R, Alhelou HH. Performance and reliability improvement of partially shaded PV arrays by one-time electrical reconfiguration. *IEEE Access*. 2022;10:46911-46935. doi:10.1109/ACCESS.2022.3171107
50. Raj RDA, Naik KA. Priority queue-based switching matrix algorithm for adaptive neuro-fuzzy inference system assisted MPPT controlled PV system. *Energ Conver Manage*. 2023;293:117519, ISSN 0196-8904. doi:10.1016/j.enconman.2023.117519
51. Bagkavos D, Patil PN. Improving the Wilcoxon signed rank test by a kernel smooth probability integral transformation. *Stat Probab Lett*. 2021;171:109026, ISSN 0167-7152. doi:10.1016/j.spl.2020.109026

How to cite this article: Naik KA, Raj RDA, Babu TS, Aljafari B. Enhancement of photovoltaic array characteristics and global maximum power using Padovan transform-based image encryption strategy. *Int J Circ Theor Appl*. 2024;52(7):3532-3557. doi:10.1002/cta.3914

APPENDIX A

TABLE A1 Parameters of the KC175GT module.

Maximum power	175 W
Maximum power current	7.42 A
Maximum power voltage	23.6 V
Short-circuit current	8.09 A
Open-circuit voltage	29.2 V
Cells per module	48

TABLE A2 Specifications of the modules used in experimental validation of proposed reconfiguration strategy in Section 4.3.

Maximum power	3 W
Maximum power current	0.34 A
Maximum power voltage	9.01 V
Short-circuit current	0.38 A
Open-circuit voltage	10.8 V

TABLE A3 Specifications of the overall PV system used in experimental validation of the combined reconfiguration-MPPT controller in Section 4.4.

PV module	10 W_p
PV array (5 × 5 array)	250 W_p
Switching frequency	5000 Hz
Load resistance	159.2 Ω
Boost capacitor	6.5 μF
Boost inductor	2.01 mH
DC link capacitor	500 μF